

# **Radionuclide Migration at the Gasbuggy Underground Nuclear Test Site**

prepared by

Clay A. Cooper and Jenny B. Chapman

Division of Hydrologic Sciences  
Desert Research Institute  
Nevada System of Higher Education

submitted to

S.M. Stoller Corporation  
U.S. Department of Energy  
Office of Legacy Management  
Grand Junction, Colorado

August 2015

**Publication No. 41262**

Reference herein to any specific commercial product, process, or service by trade name, trademark, manufacturer, or otherwise, does not necessarily constitute or imply its endorsement, recommendation, or favoring by the United States Government or any agency thereof or its contractors or subcontractors.

Available for sale to the public from:

U.S. Department of Commerce  
National Technical Information Service  
5301 Shawnee Rd.  
Alexandria, VA 22312  
Phone: 800.553.6847  
Fax: 703.605.6900  
Email: [orders@ntis.gov](mailto:orders@ntis.gov)  
Online ordering: <http://www.osti.gov/ordering.htm>

Available electronically at <http://www.osti.gov/bridge>

Available for a processing fee to the U.S. Department of Energy and its contractors, in paper, from:

U.S. Department of Energy  
Office of Scientific and Technical Information  
P.O. Box 62  
Oak Ridge, TN 37831-0062  
Phone: 865.576.8401  
Fax: 865.576.5728  
Email: [reports@adonis.osti.gov](mailto:reports@adonis.osti.gov)

# **Radionuclide Migration at the Gasbuggy Underground Nuclear Test Site**

prepared by

Clay A. Cooper and Jenny B. Chapman

Division of Hydrologic Sciences  
Desert Research Institute  
Nevada System of Higher Education

Publication No. 41262

submitted to

S.M. Stoller Corporation  
U.S. Department of Energy  
Office of Legacy Management  
Grand Junction, Colorado

August 2015

---

The work upon which this report is based was supported by the U.S. Department of Energy under a subcontract to Prime DOE Contract #DE-AM01-07LM00060. Approved for public release; further dissemination unlimited.

**THIS PAGE INTENTIONALLY LEFT BLANK**

## EXECUTIVE SUMMARY

The U.S. Department of Energy, under its former name the Atomic Energy Commission, conducted a program in the 1960s and 1970s that evaluated technology for the nuclear stimulation of low-permeability natural gas reservoirs. The first project in the program, Project Gasbuggy, was located in Rio Arriba County in northwest New Mexico. A 29-kiloton nuclear device was detonated 1,292 m below the land surface on December 10, 1967 in the Lewis Shale. The detonation resulted in the formation of a slump- and rubble-filled chimney extending from 40 m below the detonation to the contact between the Pictured Cliffs Sandstone and overlying Fruitland Formation. The chimney radius was estimated as 25 m, with explosion-generated fractures extending 120 to 150 m in all directions. The detonation generated radionuclides from residual fuel products, nuclear reactions, and activation products. Most of the radionuclides are contained in the solidified melt glass, but several gaseous radionuclides were detected in produced gas from testing of the emplacement hole that occurred in 1968 and 1969. Of the three important gas radionuclides, the majority of  $^{14}\text{C}$  and  $^{85}\text{Kr}$  were flared to the atmosphere during testing, but tritium—being able to exchange with hydrogen and therefore able to form liquid water (and vapor)—remained in the subsurface in large quantities. The test produced an estimated 40,000 Ci of tritium, present primarily in the form of tritiated water (HTO).

The overarching objective of this analysis of Gasbuggy is to develop a model that can be used to support strategic planning for long-term surveillance and maintenance of the Gasbuggy site. The first specific objective of this work is to understand the likely extent of tritium in the subsurface around the Gasbuggy test location at the present day. This is met by estimating the distance tritium has migrated from the chimney in the 47 years since the detonation. A conceptual flow and transport model around the emplacement hole (GB-ER) was developed to investigate tritium transport rates in the subsurface. The conceptual model was implemented into the TOUGH2 computer program, which is capable of simulating (radioactively) decaying tritium migrating advectively and diffusively in both gas (in this case as water vapor mixed with methane) and aqueous phases (liquid water). Results demonstrate that for the conditions modeled, HTO diffuses in the gas phase 110 m from the location of the detonation after 47 years. Although HTO is able to exchange phases from gas to liquid and back again, the faster-diffusing gas phase (by four orders of magnitude) is responsible for most of the tritium transport away from the chimney.

The second specific objective is to examine how close new natural gas wells could be drilled and extract gas from the Pictured Cliffs Sandstone without producing tritium from the Gasbuggy test. The conceptual model was adjusted to include a single producing gas well, located 340 m from the detonation point, along the direction of maximum principal stress. Fluid flow should be enhanced in the maximum principal stress direction as a result of well stimulation techniques such as hydraulic fracturing. The hypothetical gas well produced 2.3 BCF of gas over 30 years, on deliverability, from a 10-m interval located in the middle of the Pictured Cliffs Sandstone, at nearly the same elevation as the detonation. The results show that the drainage radius reaches the nuclear chimney within the first few years of production, but that the gas-phase velocities are not high enough to allow HTO to reach the well.

Effort was made to ensure that the calculation processes were conservative, that is, when uncertain, to use parameter values that promote tritium transport. The subsurface formations affected by the Gasbuggy test, the Lewis Shale and Pictured Cliffs Sandstone, were formed during large transgressive and regressive marine cycles, leading to more uniform (and more predictable) flow and transport properties than other, more complex sedimentary environments such as streams or deltas. Fracture properties within these formations, however, are poorly understood and their geometry and flow properties are complicated. Recognizing this uncertainty, parameter values for permeability, porosity, and tortuosity of the fractured zones were selected to favor transport of tritium toward the producing well.

## **ACKNOWLEDGMENTS**

This work benefited from the knowledge and insight provided in conversations by Rex Hodges, Rick Hutton, and Jeff Price (all at S.M. Stoller Corp.); Jim Lovato (BLM); Paul Marusak (ConocoPhillips); and Jalena Dayvault (DOE). We also thank Lisa Wable for drawing several of the figures.

## CONTENTS

EXECUTIVE SUMMARY .....	iii
LIST OF FIGURES .....	vi
LIST OF TABLES .....	vii
1.0 INTRODUCTION .....	1
1.1 Physical Description of Site.....	1
1.2 Gasbuggy Test Operations.....	4
1.3 Radionuclides of Potential Concern.....	6
1.4 Objective and Scientific Approach.....	7
2.0 EXPLOSION PHENOMENOLOGY AND CONCEPTUAL MODEL OF FLOW AND TRANSPORT .....	8
2.1 Explosion Phenomenology .....	8
2.2 Conceptual Flow Model.....	9
2.3 Conceptual Transport Model .....	10
3.0 FORMULATION OF THE NUMERICAL MODEL.....	12
3.1 Choice of Numerical Simulator .....	12
3.2 Model Domain .....	12
3.3 Boundary Conditions .....	14
3.4 Flow Model Parameters .....	14
3.4.1 Liquid and gas properties.....	14
3.4.2 Rock properties .....	16
3.4.2.1 Intrinsic permeability.....	16
3.4.2.1.1 Nuclear cavity and chimney .....	16
3.4.2.1.2 Nuclear-stimulated zone.....	16
3.4.2.1.3 Pictured Cliffs Sandstone .....	17
3.4.2.1.4 Fruitland Formation and Lewis Shale .....	17
3.4.2.1.5 Hydraulic fracture zone.....	17
3.4.2.2 Porosity, saturation, capillary pressure, and relative permeability.....	18
3.4.2.2.1 Porosity of the nuclear chimney.....	18
3.4.2.2.2 Porosity of all other rock types .....	18
3.4.2.2.3 Phase saturation.....	18
3.4.2.2.4 Capillary pressure.....	18
3.4.2.2.5 Relative permeability .....	19
3.5 Transport model parameters .....	21
3.5.1 Chemical transport properties .....	21
3.6 Radioactive Source Values .....	22
3.7 Transient parameters.....	22
3.7.1 Gas well production characteristics .....	22

3.7.2	Hydraulic fracture zone geometry .....	24
3.8	Partial Model Calibration to Nuclear Chimney .....	24
4.0	MODEL RESULTS .....	25
4.2	Tritium Migration during Gas Production .....	28
5.0	CONCLUSIONS.....	32
6.0	REFERENCES .....	35

## LIST OF FIGURES

1.	Location of the Gasbuggy site, New Mexico (from DOE, 2002).....	2
2.	Generalized cross section of the San Juan Basin. From Stone <i>et al.</i> (1983).....	3
3.	Diagrammatic cross section of the formations intersected by the Gasbuggy emplacement hole. ....	4
4.	Locations of boreholes drilled for the Gasbuggy Project and Well EPNG 10-36.....	5
5.	“Artist’s conception” of vertical cross section through the Gasbuggy chimney and nearby boreholes .....	9
6.	Computation domain showing boundary conditions on all six sides, location of chimney and hypothetical production well .....	13
7.	Cross section of model domain: the bottom 100 m of Ojo Alamo Sandstone, Kirtland Formation, and Fruitland Formation overlies the 90 m high Pictured Cliffs Sandstone, which overlies the top 160 m of the Lewis Shale.....	13
8.	Capillary pressure curves from six cores (circles) from the Pictured Cliffs Sandstone and best fit (blue) through the majority of the data .....	19
9.	Data used for relative permeability (squares) to gas and the van Genuchten (1980) fit used for the model (green) for the Pictured Cliffs Sandstone .....	20
10.	Relative permeability curves to gas (green) and liquid water (blue) for the nuclear chimney and detonation-induced fractures. ....	21
11.	Gas produced, in thousand cubic feet, for three wells (colors) and the simulation (black circles).....	23
12.	Bottom hole pressure as a function of time (red squares) from the 15-day production test in 1968 and subsequent recovery over the following four months .....	25
13.	Initial mass fraction of tritium in the <b>gas</b> phase ( $X_g^{HTO}$ or tritiated water vapor) in December 1967 at the start of the simulation .....	26
14.	Mass fraction of tritiated water vapor in 1993, 26 years after the detonation. ....	27
15.	Mass fraction of tritiated water vapor in 2014, 47 years after the detonation. ....	27
16.	Mass fraction of tritiated <b>liquid</b> water in 2014, 47 years after the detonation .....	28
17.	Map view of mass fraction of tritiated water vapor (color flood) and pressure (black contours) after three years of production .....	29
18.	Mass fraction of tritiated water vapor in 2022, 55 years after the detonation and 8 years after the start of gas production from a hypothetical well (red vertical line) located 340 m from the detonation .....	29
19.	Mass fraction of tritiated water vapor after 18 years of gas production, in the year 2032.....	30

20.	Mass fraction of tritiated water vapor after 28 years of gas production, in the year 2042.....	30
21.	Mass fraction of tritiated water vapor after 30 years of gas production, in the year 2044.....	31
22.	Mass fraction of tritiated water vapor 120 years after the detonation, in the year 2087, 43 years after gas production has ceased. ....	31
23.	Map view of mass fraction of tritiated water vapor (color flood) and pressure (black contours) after three years of production for a deliverability pressure of 800 psi (5.5 MPa) from a well located 400 m from the working point .....	32

### LIST OF TABLES

1.	Input data for the simulations. ....	15
----	--------------------------------------	----

### ABBREVIATIONS

AEC	U.S. Atomic Energy Commission
BCF	billion cubic feet (of gas)
<sup>14</sup> C	carbon-14
Ci	Curie
DOE	U.S. Department of Energy
EPM	equivalent porous medium
ft	feet
H	hydrogen atom
He	helium atom
<sup>3</sup> H	tritium atom
HTO	tritiated water molecule
IC	Institution Control
<i>k</i>	intrinsic permeability
<i>k<sub>rl</sub></i>	relative permeability to liquid (or <i>g</i> , to gas)
<sup>85</sup> Kr	krypton-85
L	Length
LS	Lewis Shale
m	meters
M	mass
md	millidarcy

MPa	Megapascals (1 million Pa)
NNSS	Nevada National Security Site
<i>P</i>	pressure
Pa	Pascals
PI	Productivity Index
psi	pounds per square inch
MCFD	thousand cubic feet (of gas) per day
MMCFD	million cubic feet per day
PC	Pictured Cliffs Sandstone
<i>S</i>	saturation
STP	standard temperature and pressure
<i>t</i>	time
T	tritium atom

### **Subscripts and Superscripts**

<i>g</i>	gas
<i>l</i>	liquid
<i>r</i>	residual, as in residual saturation; relative, as in relative permeability
HTO	tritiated water

### **CONVERSIONS**

$$1 \text{ m} = 3.281 \text{ ft}$$

$$1 \text{ md} = 9.87 \times 10^{-16} \text{ m}^2 \sim 10^{-15} \text{ m}^2$$

$$1 \text{ psi} = 6,891 \text{ Pa}$$

$$1 \text{ MMCFD gas} = 0.3736 \text{ kg sec}^{-1} \text{ gas for gas density } 1.14 \text{ kg m}^{-3}$$

## **1.0 INTRODUCTION**

The U.S. Department of Energy (DOE), under its former agency names as well as its current name, is responsible for underground testing of nuclear weapons and devices as part of research and development for the national defense. The DOE is committed to managing responsibilities associated with the environmental legacy of these activities. The DOE Office of Legacy Management is specifically responsible for ensuring the DOE's responsibilities are met for the Gasbuggy site and for providing effective and efficient long-term surveillance and maintenance to protect human health and the environment. The Gasbuggy site is located in northern New Mexico, approximately 100 miles northwest of Santa Fe. Gasbuggy was part of an investigation into peaceful uses of nuclear devices under the Plowshare program. Several of these Plowshare tests, including the Gasbuggy test, were conducted in an attempt to increase natural gas production of low-permeability reservoirs. The device had an announced yield of 29 kilotons (DOE, 2000) and was detonated 1,292 meters (m) (4,240 feet) below ground surface on December 10, 1967.

The overarching objective of this report is to develop a model that can be used to support strategic planning for long-term surveillance and maintenance of the Gasbuggy site. Specifically, the purpose is to estimate the extent of radionuclide contamination in the subsurface at the present day and to forecast radionuclide migration during possible future production of natural gas from nearby wells. This introduction continues with a physical description of the site, a brief history of site operations, and previous work and background specific to recent site activities. The body of the report describes the development of a conceptual model for subsurface gas and liquid flow and radionuclide migration, followed by the implementation of this model into a numerical simulator to quantitatively estimate the fate of radionuclides in time and space. The results, and associated uncertainty, are discussed with the goal of providing information for decision makers to consider for site management.

### **1.1 PHYSICAL DESCRIPTION OF SITE**

The Gasbuggy site is in Rio Arriba County within the Carson National Forest, Jicarilla Ranger District (Figure 1). The Jicarilla Apache Indian Nation lies one mile to the east. The Gasbuggy site is generally considered to be the southwest quarter of Section 36, Township 29 North, Range 4 West, New Mexico Principal Meridian, though there were at least five operational areas during site activities and some of these were outside the quarter section.

The site is located within canyon and plateau topography typical of the Colorado Plateau Physiographic Province. Elevations range from 2,100 to 2,200 m (7,000 to 7,300 ft) above sea level in the immediate area and the elevation at surface ground zero is 2,179 m (7,149 ft). Three vegetation communities are supported at the site: Rocky Mountain Montane Conifer Forest, Great Basin Mountain Scrub, and Great Basin Grassland (Shrub-Grassland Sagebrush Grass Series and Shrub-Grassland Wheatgrass Series). There are no streams, springs, or seeps on the site. Ephemeral drainages lead to La Jara Creek.

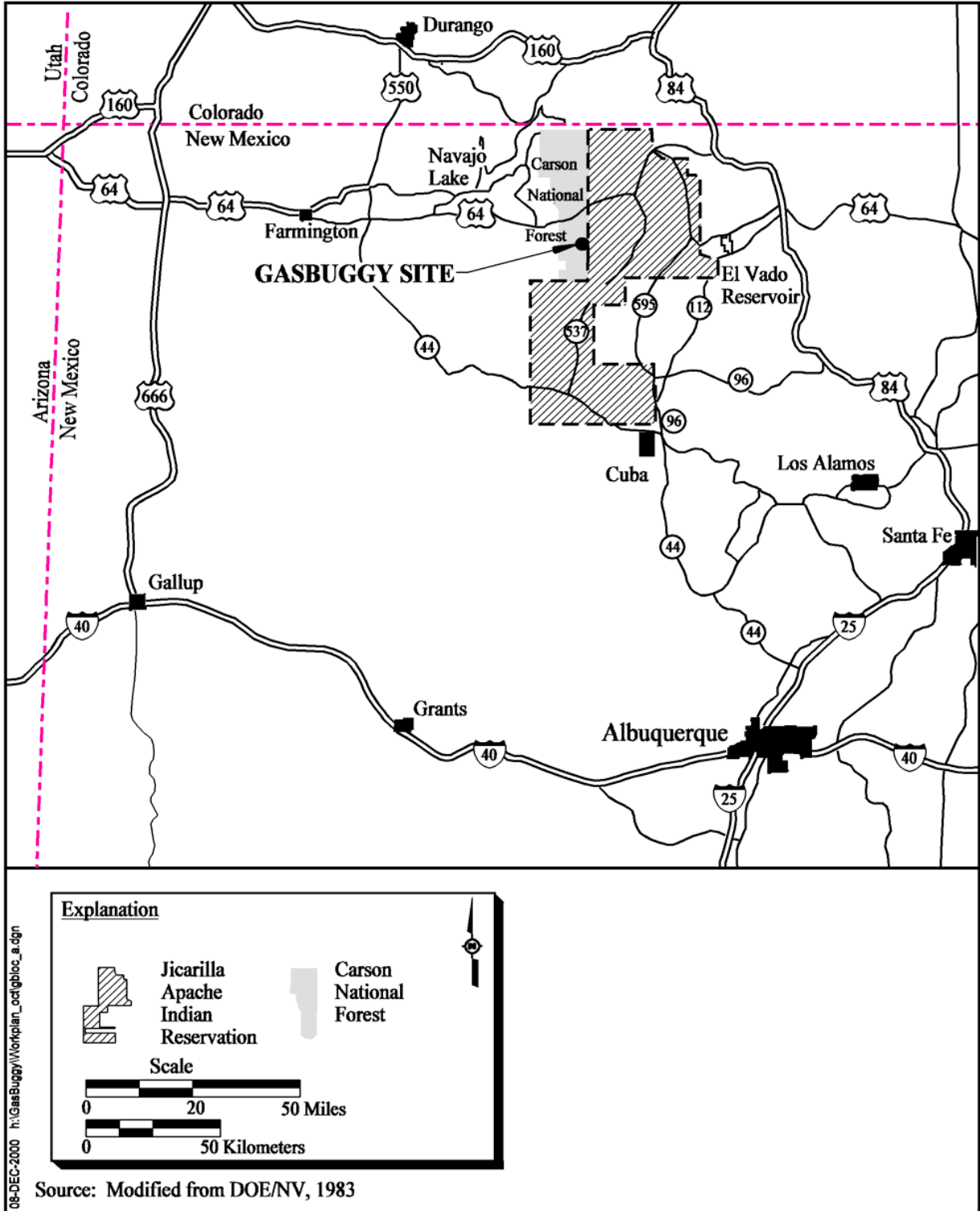


Figure 1. Location of the Gasbuggy site, New Mexico (from DOE, 2002).

Geologically, Gasbuggy is located in the San Juan Basin, a large structural basin containing approximately 3,700 m (12,000 ft) of sedimentary rocks (Figure 2). The nuclear test was detonated in the upper part of the Cretaceous Lewis Shale Formation with the intention of fracturing the overlying Pictured Cliffs Sandstone Formation (Figure 3). The Lewis Shale extends another 450 m (1,500 ft) vertically below the test. The Pictured Cliffs is one of the San Juan Basin's major gas reservoirs. However, in the northeast part of the basin where Gasbuggy is located, the Pictured Cliffs is a low-productivity, sparsely developed reservoir with a thickness of about 90 m (300 ft).

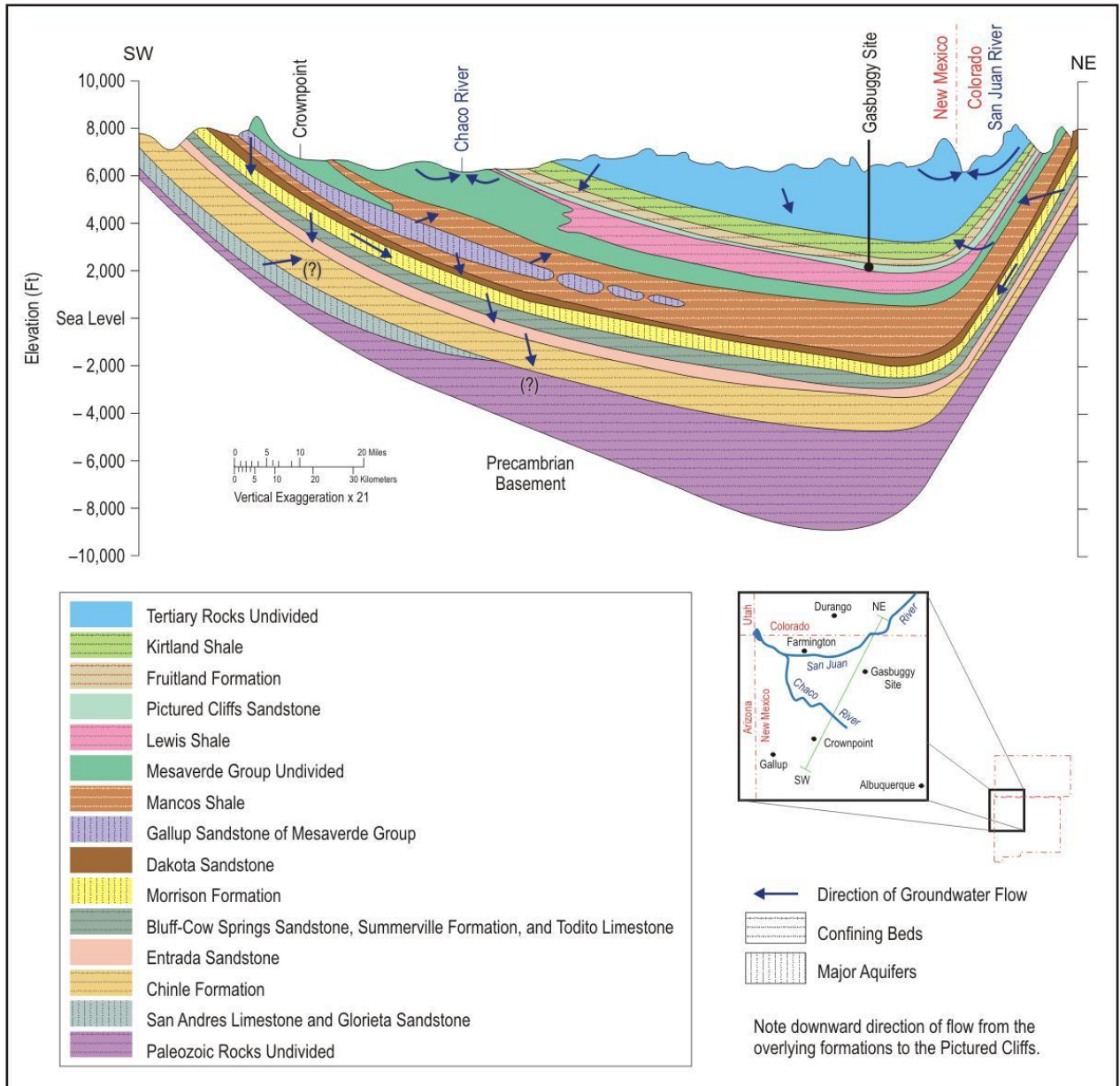


Figure 2. Generalized cross section of the San Juan Basin. From Stone *et al.* (1983). Arrows depict direction of groundwater flow.

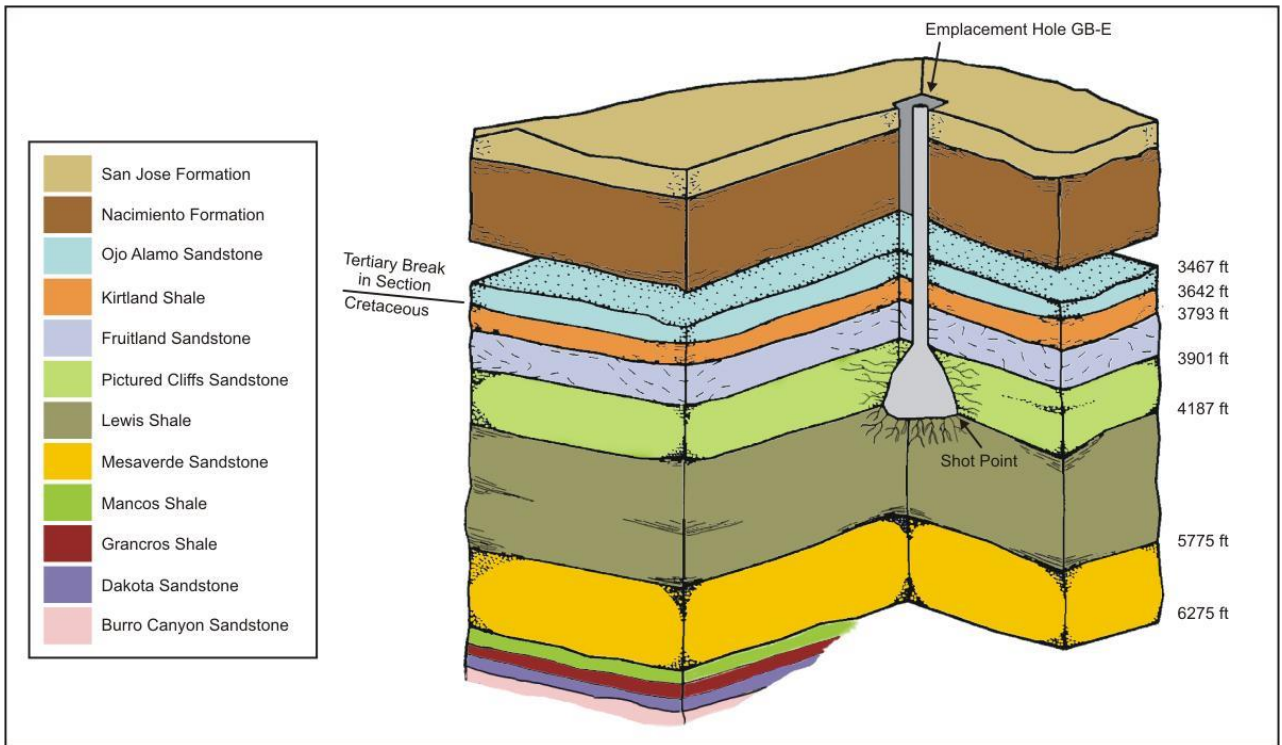


Figure 3. Diagrammatic cross section of the formations intersected by the Gasbuggy emplacement hole.

Overlying the Pictured Cliffs is the 30-m-thick (100-ft) Fruitland Formation, composed of sandstone, siltstone, shale, and coal. The Kirtland Shale overlies the Fruitland Formation. The Ojo Alamo Sandstone is above the Kirtland Shale and was identified as the closest water-bearing unit to the test horizon. The Ojo Alamo is a fine- to medium-grained, clayey sandstone containing minor shale beds (Mercer, 1967). Above the Ojo Alamo is the Nacimiento Formation, which is overlain by the San Jose Formation. The Nacimiento and San Jose are continental floodplain deposits with a combined thickness of approximately 1,050 m (3,500 ft). The fine- to medium-grained sandstone, interbedded with claystone and shale is water-bearing in many parts of the basin. Several tens of feet of alluvium (silty sand, poorly graded sand, and silt) occur at land surface in the immediate site vicinity.

Water supply wells in the general area tap both the alluvium and the underlying sandstones at depths between 16.5 and 70 m (54 and 229 ft) (Mercer, 1968). Drilling during surface cleanup investigations did not identify shallow groundwater in boreholes as deep as 22.5 m (74 ft) around the emplacement well, though groundwater was encountered in boreholes as shallow as 17.5 m (58 ft) near Well GB-D to the southeast (DOE, 2004).

## 1.2 GASBUGGY TEST OPERATIONS

The rationale and basic plan for the Gasbuggy project was presented in a feasibility study (El Paso Natural Gas *et al.*, 1965) prepared by El Paso Natural Gas, the U.S. Atomic Energy Commission (predecessor to DOE), the U.S. Department of Interior's Bureau of Mines, and Lawrence Radiation Laboratory. One natural gas production well existed at the proposed site, EPNG 10-36, which is also known as San Juan 29-4 Unit 10. It was drilled in

1956 and was in continuous production until 1966, producing a total of 82 million cubic feet of gas. Exploratory work at the site began in 1967. The exploratory wells GB-1 and GB-2 provided data that led to site acceptance and drilling of the GB-E nuclear emplacement hole (Figure 4). All wells were plugged prior to the nuclear test. On December 10, 1967, a 29-kiloton nuclear explosive was detonated at a depth of 1,292 m (4,240 ft) in GB-E.

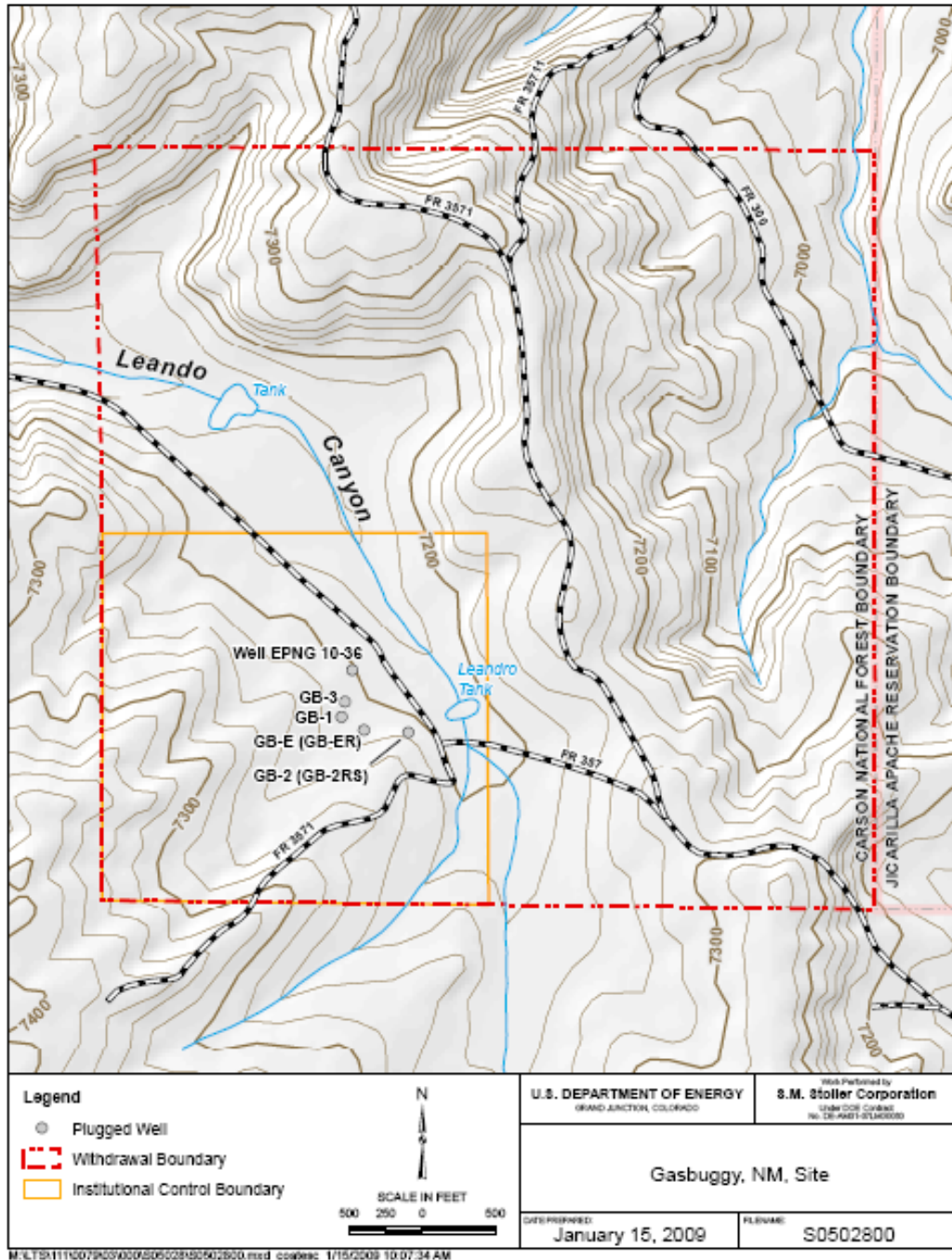


Figure 4. Locations of boreholes drilled for the Gasbuggy Project and Well EPNG 10-36. The distance from GB-E to 10-36 is 132 m (433 ft).

After the nuclear test, GB-E, GB-2, and EPNG 10-36 were reentered to provide access for production testing. The reentered GB-E was renamed GB-ER. Six major production tests were conducted in GB-ER to evaluate the nuclear stimulation. A 15-day production test began on June 28, 1968. On November 4, 1968, a series of three 30-day production tests began, followed by a 7-month production period, each at successively lower pressure. The 7-month test began in March 1969 and ended in October. A final pressure drawdown test occurred in November 1969, after which the well was shut in.

The casing in GB-2 was collapsed and a sidetrack hole (GB-2RS) was drilled out of it. A new hole, GB-3, was also drilled after the nuclear test. Borehole collapse around the production tubing prevented production testing in GB-2RS, though limited production and flow-meter data were collected during drilling. Well GB-3 was drilled in August and September 1969. Production testing was apparently not conducted in GB-3, though limited production and flow-meter data are available from drilling and completion activities. Reentry into EPNG 10-36 encountered damaged casing that prevented cleaning out the stemming material to the depth of the Pictured Cliffs. This resulted in recompletion of the well in the Ojo Alamo Sandstone.

### 1.3 RADIONUCLIDES OF POTENTIAL CONCERN

Radionuclides associated with an underground nuclear test are present in three basic forms: gases, surface deposits, and volume deposits (Smith *et al.*, 1995), the proportions of which change with time after the detonation. Immediately after the detonation, essentially all of the radionuclides are part of a superheated, expanding gas (Borg *et al.*, 1976). When the temperature and pressure begin to drop, many of the gases condense. The condensation occurs based on the boiling point of the nuclide. The refractory (high boiling point) species are primarily trapped in the solidifying melt glass<sup>1</sup>, much of which collects at the base of the cavity as “puddle glass.” These are the volume deposits, whose release from the solid phase is controlled by dissolution of this glass. Volatile (low boiling point) nuclides remain as gases longer, depending on the cooling rate of the cavity. Some portion of volatiles is embedded in the puddle glass, but a portion is also deposited as coatings on chimney rubble surfaces. These surface deposits are more susceptible to dissolution by groundwater than the puddle glass. Once dissolved in groundwater, surface and volume deposited radionuclides react with aquifer minerals, often exhibiting strong sorption properties that retard their movement.

Both liquid water and gas (primarily methane and water vapor) exist in the pore space of the Lewis Shale, Pictured Cliffs Sandstone, and Fruitland Formation. This two-phase (liquid and gas) environment, coupled with a slow glass dissolution rate and strong sorptive properties, lead to the volume- and surface-deposited radionuclides not being considered to pose a risk through a groundwater pathway at the Gasbuggy site. These contaminants could pose a risk if materials from the cavity were brought to the surface, necessitating the existing drilling restriction surrounding the nuclear cavity through perpetuity.

Of the gaseous radionuclides produced from the detonation, tritium (T or <sup>3</sup>H), <sup>85</sup>Kr, and <sup>14</sup>C are of most interest. Other gas compounds such as <sup>37</sup>Ar, <sup>39</sup>Ar, and <sup>131</sup>I were either produced in such small amounts or have shorter half-lives that they would become

---

<sup>1</sup> Molten rock that has cooled rapidly and has an amorphous, rather than crystalline, structure.

insignificant several months after the detonation (Smith, 1970; Tewes, 1979). The total amount of tritium released from the nuclear test was estimated as about 40,000 Ci (Curies; Tewes, 1979). There is no uncertainty given for this initial tritium estimate, therefore we estimate the initial radioactivity to be accurate to half of the magnitude of the least significant digit, in this case, half of 10,000. With this consideration, the initial estimate of tritium release is 35,000–45,000 Ci.

Of the total tritium amount, 2,500 Ci was estimated to be initially present in the dry gas phase (Holzer, 1970). This includes tritium included as part of the methane molecule (CH<sub>4</sub>) and other hydrocarbons, as well as tritiated hydrogen gas. Virtually all of the CH<sub>4</sub> and HT in dry gas were removed from the subsurface during gas testing and flaring between 1968 and 1972 (Tewes, 1979). A total of 2,432 Ci of tritium was released to the environment during testing, along with slightly over 7 Ci of liquid tritium disposed of off-site (AEC, 1971). The tritium production values, with or without the water portion, are within the estimated uncertainty of the original release. At present day, due to decay, there are approximately 2,830 Ci of tritium in the subsurface, with the range between 2,476 and 3,184 Ci based on the original 35,000 and 45,000 Ci range discussed above.

Smith (1970) measured the total amount of <sup>85</sup>Kr generated by the nuclear test as 350±20 Ci (by comparing concentrations to a known amount of a tracer added to the device before detonation). This amount is consistent with preshot estimates of <sup>85</sup>Kr production based on expected device performance. Virtually all of the <sup>85</sup>Kr was removed from the subsurface during the production testing. Through November 1969, 364 Ci of <sup>85</sup>Kr were released to the environment, as recorded by a monitoring system on the flaring line (AEC, 1971). Holzer (1970) calculated that approximately 7 Ci of <sup>85</sup>Kr remained in the subsurface at the end of October 1969, a value that would be less than 0.4 Ci in 2014.

The total amount of <sup>14</sup>C initially generated from the detonation is not publicly available. However, the amount produced during testing is estimated as 10.27±0.9 Ci (Tewes, 1979). Approximately 7.19±1.54 was flared during testing in 1968–1970; the remaining was accounted for as an “integrated release during all production.” The majority of <sup>14</sup>C produced was <sup>14</sup>CO<sub>2</sub> (approximately 85 percent) as compared to <sup>14</sup>CH<sub>4</sub> (15 percent) (see Table 10 in Tewes, 1979). Jacobs *et al.* (1971) report that approximately 0.5 Ci of <sup>14</sup>C remained available for production from GB-ER in late August 1969. The long half-life (5,730 yr) of <sup>14</sup>C would result in essentially the same amount in the subsurface at present day.

#### 1.4 OBJECTIVE AND SCIENTIFIC APPROACH

The objective of this work is to develop a quantitative, predictive model to estimate the extent of radionuclide movement (primarily tritium) away from the detonation zone. This information will support site stewardship to protect human health and the environment. The model represents radionuclide migration during two periods. The first period is an estimation of the extent of tritium migration in the subsurface from the nuclear detonation to present (2014) because it is affected by the permeability and effective porosity<sup>2</sup> of the geologic formations, diffusion characteristics, and radioactive decay. The second period follows the first and estimates tritium migration as influenced by production of gas from a nearby well with the aim of determining the minimum distance a gas production well, producing from the

---

<sup>2</sup> In this report, porosity implies effective porosity, which does not include isolated pores.

same horizon as the nuclear detonation, could be located and not intercept radionuclides. Because of the complexities involved in the calculations, the equations are solved using a computer program capable of simulating multiphase (gas and liquid) flow, and radionuclide (tritium in both phases) transport in three dimensions. The resulting model depicts tritium concentration in space and time, based on all available data.

Much of the data used in the model are from U.S. Government and industry reports documenting studies at the Gasbuggy location between 1967 and 1973. Most of the studies done prior to the nuclear detonation were to characterize the subsurface in terms of its geologic, hydrologic, and hydraulic properties (i.e., porosity, permeability, and relative permeability of the geologic formations), whereas the postdetonation studies relate to the characterization and behavior of the reservoir as modified by the test. In addition to these data, values of parameters not specific to the Gasbuggy site (diffusion coefficients and thermal properties of rocks) were gathered from peer-reviewed literature and the New Mexico Energy, Minerals and Natural Resources Department (<http://www.emnrd.state.nm.us/>). Additionally, some of the information was corroborated by personal communication with ConocoPhillips personnel.

## **2.0 EXPLOSION PHENOMENOLOGY AND CONCEPTUAL MODEL OF FLOW AND TRANSPORT**

### **2.1 EXPLOSION PHENOMENOLOGY**

The nuclear device was detonated at a depth of 1,292 m (4,240 ft) below ground surface. The resulting heat vaporized rock and created a void (cavity) with a radius of 25 m (Figure 5; Rawson *et al.*, 1968)<sup>3</sup>. The formation of the cavity meant that some overburden rock was no longer supported. Within 30 seconds of the detonation, geophones detected the collapse of the overburden into the cavity, resulting in a rubble-filled chimney (Smith, 1970). The pressure wave from the detonation exceeded lithostatic pressure radially 146 m from the working point, which fractured the surrounding rock. This is based primarily on the fact that a cable break in GB-1, located 146 m radially from the shot point, was most likely caused by the detonation (the predicted fracturing radius was 130 m). The chimney is thought to extend vertically from 28 m below the working point to 100 m above, to the top of the Pictured Cliffs. Although the bottom of the chimney is uncertain, postshot drilling (GB-ER) strongly supports the elevation of the top of the chimney.

Reentry drilling began December 12, 1967, two days after the detonation, and was terminated at a total depth of 1,194 m (3,916 ft) on January 10, 1968. Two voids were encountered during drilling, one between 1,175 and 1,177 m and the second between 1,191 and 1,194 m. At this point, the drill bit encountered broken steel casing sheared from the test. After 20 minutes, radioactive xenon was detected at the land surface, suggesting that communication with the chimney had been established (Holzer, 1968). This is contradicted by the short-term flow tests that resulted in rapid pressure decline, suggesting that GB-ER was not in communication with the chimney (Korver and Rawson, 1968). The initial pressure recorded was 2.3 MPa (Korver and Rawson, 1968) but increased to 5.7 MPa within several days and remained there for the following two months. A maximum downhole temperature of 66°C was recorded seven days after drilling was completed.

---

<sup>3</sup> This was updated from an earlier report by Korver and Rawson (April, 1968), which stated that the radius was 150 ft (45.7 m).

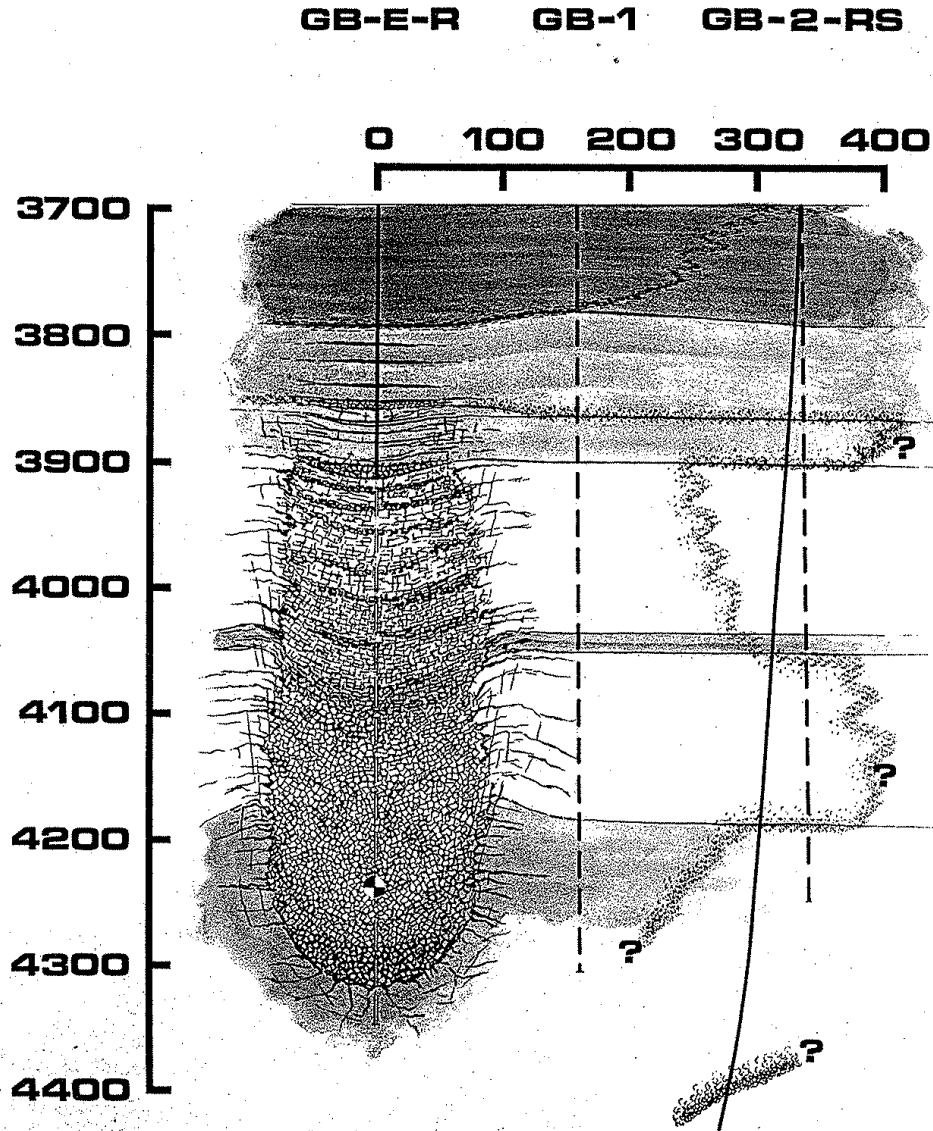


Figure 5. “Artist’s conception” of vertical cross section through the Gasbuggy chimney and nearby boreholes. Distances (in feet) were determined from postshot explorations (Rawson *et al.* 1968). The meaning of the shaded lines indicated by question marks is unknown.

## 2.2 CONCEPTUAL FLOW MODEL

Pore fluids in the Lewis Shale, Pictured Cliffs, and Fruitland Formation are about equally divided (by volume) between water and natural gas. The primary component of gas is methane, with progressively lesser amounts of higher-chained petroleum compounds (butane, ethane, pentane, etc.). Water vapor is also a significant component of gas. The intrinsic permeability of the rock matrix (the pore space, excluding fractures) is so small that gas production is infeasible without artificially fracturing the rock. Therefore, most of the gas flow is through the slightly more permeable natural fractures, as well as fractures created

during development of the reservoir. Each phase<sup>4</sup> is assumed to be continuous throughout the reservoir and capable of flowing in response to a gradient in its potential energy (PE), where PE is the sum of the gravitational and pressure potentials of each phase. The energy gradient is quantified as a gradient in total pressure, where the pressure of a fluid is a measure of the quantity of energy per unit volume of fluid. Total pressure gradients of the two phases are not independent of one another and are coupled through capillary pressure, which is the difference in pressure between the gas and liquid phases where the two are in contact.

Petroleum does not move in response to regional pressure gradients in the same manner as groundwater because it is often trapped by geologic structures such as folds or faults (structural traps), changes in lithology (stratigraphic traps), or by differences in the pressure gradients of the petroleum and underlying groundwater in the presence of a lithologic change. The general idea is that gas dissolved in moving groundwater will come out of solution and form a separate buoyant phase when its partial pressure exceeds the pressure of the water, eventually becoming trapped when structural or stratigraphic conditions are met. However, these traps also contain significant amounts of water held in place largely by capillary forces.

In the natural state, unaffected by the nuclear detonation, gas flow is predominantly through joints, fractures, and bedding planes of the Pictured Cliffs Sandstone. The aperture of natural fractures in Pictured Cliffs Sandstone is on the order of 0.5–1 mm, which is larger than the characteristic diameter of pores in the matrix, so the more-permeable fractures are expected to be filled with the gas, while the pore spaces contain both gas and liquid phases. This distribution of phases in the rock is derived from considerations of capillarity in the Laplace-Young equation. Extensive measurements have been made on Pictured Cliffs cores, but these all depict matrix properties and not properties of the fractures. A comparison of core permeability and permeability measured from reservoir testing reveals that the cores have a higher permeability than the reservoir (Rawson *et al.*, 1968, p. 6; Ward and Lemon, 1968).

### 2.3 CONCEPTUAL TRANSPORT MODEL

The conceptual transport model can be considered in two parts. The first considers the source of the radionuclides, including the manner in which they are released, whereas the second part concerns the processes that occur as radionuclides migrate away from the source.

Radionuclides remaining after an underground nuclear test can be attributed to three sources (Borg *et al.*, 1976): (1) residual nuclear material that has not undergone a nuclear reaction (unspent fuel), (2) direct products of the nuclear reactions (fission products and tritium), and (3) activation products produced by neutron capture in the immediate vicinity of the explosion. When the nuclear device is detonated underground, the cavity is initially filled with vaporized material derived from the rock and construction materials associated with the device and emplacement hole, as well as the radionuclide components. As the cavity cools, radionuclides are distributed into four phases: (1) in the nuclear melt glass, (2) as surface deposits on rubble in the cavity and chimney, (3) dissolved in water, or (4) as part of the gas phase (IAEA, 1998).

---

<sup>4</sup> The distinction is made that gas and liquid phases are both fluids.

The total radiologic source term is not equally available for transport from the cavity. Most of the fission products are refractory (having low volatility) and are incorporated into nuclear melt glass. These will leach very slowly out of the glass as the glass itself slowly reacts with gases and liquids present in the subsurface. More volatile radionuclides, or those with a gaseous precursor (such as  $^{137}\text{Cs}$ , which is produced by the decay of  $^{137}\text{Xe}$ ), occur both in the melt glass and as more easily dissolved deposits on rock surfaces. Although surface-deposited nuclides are more readily dissolved into groundwater than those in melt glass, many are reactive and tend to sorb strongly onto mineral surfaces. Several radionuclides are almost completely mobile in groundwater, with the most significant being tritium (T or  $^3\text{H}$ ).

At Gasbuggy, the very low intrinsic permeability, coupled with approximately 50 percent gas-filled pore space, results in the liquid water phase being much less mobile than the gas phase. To the extent allowed by their solubility, radionuclides in the melt glass, in mineral phases, or sorbed onto surfaces will dissolve into the aqueous phase. Some radionuclides can exist in the gas phase and therefore have greater potential for movement. The longer-lived of these radionuclides are T,  $^{85}\text{Kr}$ , and  $^{14}\text{C}$ . Of these radionuclides present at Gasbuggy, T is by far the most abundant, as discussed previously.

It is unclear how much tritium might be trapped in the melt glass (see Cooper *et al.* [2007] for a discussion). It is assumed here that all of the tritium exists in the gas phase and that none is embedded in the melt. This is the most conservative approach, favoring tritium transport, and is consistent with source term modeling performed for underground nuclear tests at the Nevada National Security Site (NNSS) (Tompson *et al.*, 1999).

As an isotope of hydrogen, tritium can form tritiated (radioactive) water, tritiated hydrogen gas (HT), and tritiated methane (CTH<sub>3</sub>) molecules. Water exists in both gas and aqueous phases, whereas methane exists (under reservoir conditions) in only the gas phase. The pressure and temperature conditions in the Gasbuggy subsurface are not sufficient for an isotopic exchange reaction involving hydrogen to occur with methane (Frink and Wethington, Jr., 1971; Burger, 1979; Wethington, Jr., 1970). The tritiated methane observed during postdetonation gas-production testing was probably formed under the extremely high pressure and temperature conditions associated with the nuclear detonation. Due to its low solubility (22.7 mg/L in water), all tritiated methane is assumed to have been removed from the subsurface during production testing so that the majority of tritium remaining was associated with water. Similarly, atoms of tritium gas (either as T,  $^1\text{HT}$ , or T<sub>2</sub>) or as nontritiated hydrogen gas (H<sub>2</sub>) are ignored in the model. Throughout the rest of this report, “tritium” refers to tritiated water, as either a liquid or gas (vapor)<sup>5</sup>.

Tritiated liquid water is always available for partitioning when tritiated water vapor and an aqueous phase come into contact. At Gasbuggy, the aqueous phase is practically immobile and acts as a source/sink for tritium. In other words, a water vapor not containing tritium that comes in contact with tritiated liquid water will thermodynamically exchange tritiated water molecules from the aqueous to the vapor phase and vice versa.

---

<sup>5</sup> Vapor is water (tritiated or nontritiated) in the gas phase

Both diffusive and advective transport are subject to processes that retard the migration of tritiated water. One of these is the exchange that occurs between tritiated water in the aqueous and gas phases. With aqueous-phase velocities much smaller than those in the gas phase, tritiated water exchanging into the aqueous phase encounters a significantly retarded flow velocity. As tritiated water vapor migrates downgradient, it encounters tritium-free liquid water and exchange occurs, removing tritiated water from the faster (gas phase) pathway. The second significant process is radioactive decay. The tritium half-life is 12.32 years, decaying into nonradioactive helium. Therefore, as time continues, the amount of tritium mass continually decreases. This accentuates the impact of exchange because tritiated water transferred into the aqueous phase is essentially removed by decay. No other sorption or retarding processes are included in the transport model.

### **3.0 FORMULATION OF THE NUMERICAL MODEL**

#### **3.1 CHOICE OF NUMERICAL SIMULATOR**

The conceptual model includes flow and transport as fully coupled processes that must be solved simultaneously to get a realistic understanding of the spatial and temporal distribution of radionuclides within the reservoir. The Transport of Unsaturated Groundwater and Heat (TOUGH2) simulator (Pruess, 1991; Pruess *et al.*, 1999) was used to implement the flow and transport model. The TOUGH2 is a DOE-sponsored code that has been used to study heat and mass flow in geothermal reservoirs, saturated/unsaturated groundwater environments, and oil and gas reservoirs. The TOUGH2 can simulate fully coupled, transient, three-dimensional, multiphase and multicomponent nonisothermal flow. The many applications in which TOUGH2 has been applied can be found at <http://esd.lbl.gov/research/projects/tough/>. The governing equations solved by TOUGH2 are presented in the appendix. Flow through fractures is simulated using an equivalent porous medium approximation; TOUGH2 has a module capable of discrete fracture flow, but it is also based on Darcy's law (which relies on a representative continuum) and demands data for fracture characteristics (e.g., aperture, spacing, and degree of connectivity) that are largely unknown for Gasbuggy.

#### **3.2 MODEL DOMAIN**

The model is 2,000 m long in the  $x$ -direction and is 340 m thick (Figure 6). It is referenced only to the location of the nuclear chimney so that the  $x$ -direction can be viewed as being in any of the possible directions of maximum principal stress where fracturing is expected to be greatest (N35E, N55W, or NS; Lorenz and Cooper, 2003). The top of the model is located in the Fruitland Formation, 1,090 m below the land surface, and 100 m above the bottom of its contact with the Pictured Cliffs Sandstone. The domain is constructed such that the emplacement borehole GB-ER is centered in the rectangular solid comprising the chimney.

A vertical cross section of the model domain is shown in Figure 7. The nuclear chimney has a radius of 25 m with detonation-caused fractures extending from 25 m to 150 m in the Lewis Shale and 25 m to 120 m in the Pictured Cliffs. After achieving steady state flow for the time leading up to the nuclear detonation, the chimney was added, along with the detonation-associated fractures to allow tritium to diffuse radially away from the chimney. After 47 years (i.e., in 2014), the simulation was stopped, a hypothetical gas production well was placed in the domain, along with hypothetical fractures, and the model was allowed to run for an additional 100 years, until the tritium mass fraction was essentially reduced to zero everywhere in the model as a result of dilution and radioactive decay.

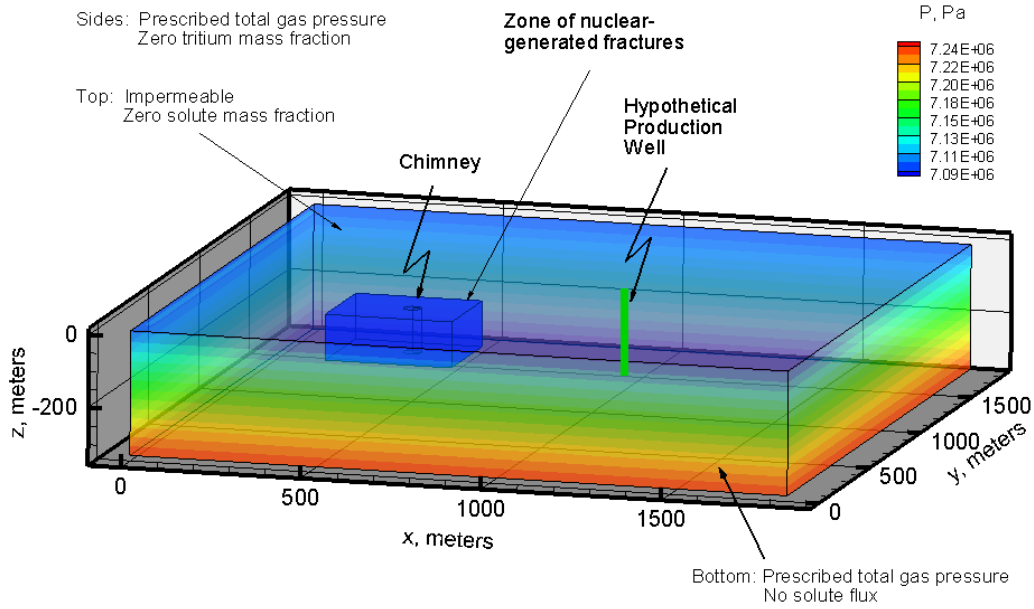


Figure 6. Computation domain showing boundary conditions on all six sides, location of chimney and hypothetical production well. The steady-state pressure field is shown in Pascals. The dimensions of the  $x$ -,  $y$ -, and  $z$ -axis are not referenced to any particular object and are relative. The top of the model is 1,090 m below ground surface. The  $x$ - direction can be considered oriented along the direction of maximum principal stress where fracturing is expected to be greatest.

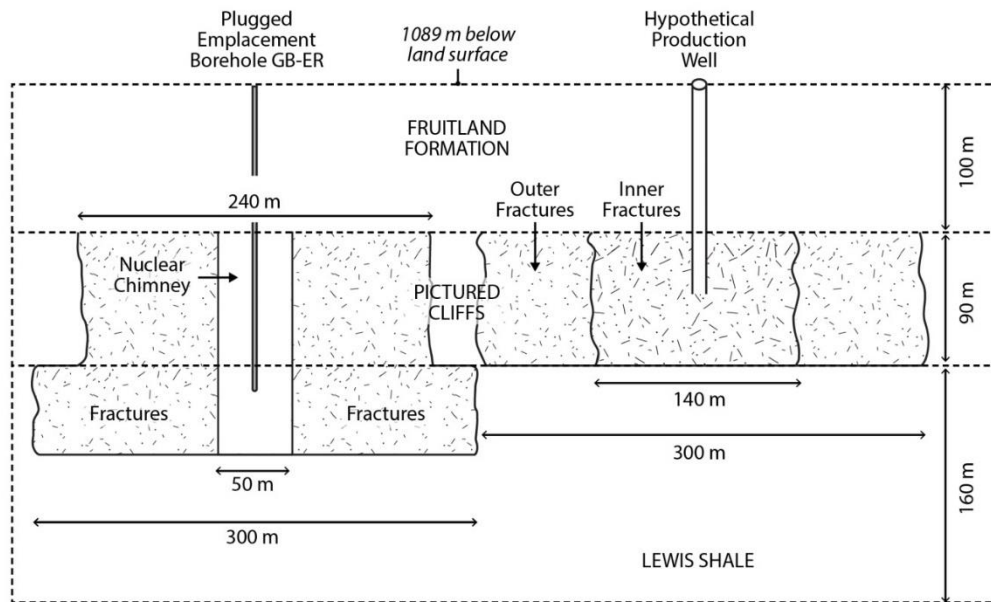


Figure 7. Cross section of model domain: the bottom 100 m of Ojo Alamo Sandstone, Kirtland Formation, and Fruitland Formation overlies the 90 m high Pictured Cliffs Sandstone, which overlies the top 160 m of the Lewis Shale. The detonation (1,292 m below the land surface) is 203 m below the top of the model domain. The lower part of the chimney occupies the upper 40 m of the Lewis Shale.

### 3.3 BOUNDARY CONDITIONS

The bottom horizontal boundary of the model is prescribed 7.24 MPa (1,050 psi; Ward and Lemon, 1968) total gas phase pressure, which remains fixed throughout each simulation. The aqueous-phase pressure is adjusted internally by TOUGH2 through the capillary pressure function. A one-dimensional vertical simulation was run to steady state to establish the corresponding pressure at the top of the domain, which is 7.10 MPa. The upper boundary was prescribed zero fluid flux, to simulate a bed of low-permeability. The thickness of the domain was set large enough such that it would be less than the distance tritium would travel vertically (through diffusion or vertical pressure gradients possibly induced by gas production at a nearby well), and therefore not constrain vertical transport. After setting the bottom boundary pressure at 7.24 MPa, all four vertical (side) boundaries bordering the computational domain were run in a separate simulation to steady state. These were then used as the initial conditions for the four vertical boundaries. The domain (2,000 m x 2,000 m x 340 m high) was made large so that the vertical boundaries would not affect flow and transport calculations around the chimney and gas production well.

At each boundary, the solute (i.e., tritium) transport boundary condition is equivalent to the respective hydraulic boundary condition. That is, zero solute concentration (as mass fraction) is prescribed in the aqueous phase on the bottom as well as each of the vertical boundaries. The top boundary is prescribed as no solute flux. Temperature effects due to chimney heat were neglected for several reasons. One is that within the first two years, the chimney temperature had dropped considerably from its highest bottom-hole temperature measurement of 120 °C on July 4, 1968 such that the reservoir had essentially reached its predetonation 54 °C temperature (Rawson *et al.*, 1968). The second reason is that when the chimney heat was present within those first few years, it would not extend much beyond the chimney, based on the thermal conduction properties of rock. For these reasons, it was decided not to include chimney heat in the model as it would extend the time of each simulation while having only a second-order effect on the tritium mass fraction field. The reservoir was assumed to be isothermal with a temperature of 54 °C.

### 3.4 FLOW MODEL PARAMETERS

All input data used in the model are presented in Table 1. Data that are site specific, such as intrinsic permeability, porosity, and initial phase saturations, were gathered from reports specific to the nuclear test as well as from published literature. Data that are not site-specific, such as diffusion coefficients, are from published sources. Some of the data—such as thermal conductivity and specific heat—are in principal site-specific but measurements were not made specific to the Gasbuggy project and their uncertainty is not critical to the model outcome.

#### 3.4.1 Liquid and gas properties

As distributed by DOE, TOUGH2 does not have the capability to model methane as the principal component of the gas phase. Modifications were therefore made to replace air with methane as the primary component of the gas phase. The modifications were to change the molecular weight of air to that of methane (16.05 g mol<sup>-1</sup>) and to change some values in the correlations used to compute dynamic viscosity. The TOUGH2 estimates viscosity based on the Chung method (Reid *et al.*, 1987), so values for the characteristic diameter of the molecule, characteristic energy, and the collision integral were replaced with values correct for methane. The parameters were taken from Appendix B of Reid *et al.* (1987). However, the steam tables, in which liquid water and water vapor partitioning in air is determined, were not modified.

Table 1. Input data for the simulations.

<b>Gas Reservoir Parameters</b>		
Parameter	Value	Source
Intrinsic permeability, $x$ -, $y$ -, $z$ -dir, Pictured Cliffs, $m^2$	$10^{-16}$	Ward and Lemon, 1968
Intrinsic perm., Fruitland Formation, $m^2$	$10^{-17}$	NM Oil & Gas <sup>1</sup>
Intrinsic perm., Lewis Shale, $m^2$	$1.5 \times 10^{-17}$	Dube <i>et al.</i> , 2000
Intrinsic perm., nuclear chimney, $m^2$	$10^{-13}$	calibrated
Intrinsic perm., explosion-generated fracture EPM, $m^2$	$10^{-14}$	calibrated
Intrinsic perm., “inner” hydraulic fractures, $m^2$	$5 \times 10^{-14}$	assumed 500k of PC
Intrinsic perm., “outer” hydraulic fractures, $m^2$	$5 \times 10^{-15}$	assumed 500k of PC
Porosity, Pictured Cliffs Sandstone	0.10	Ward and Lemon, 1968
Porosity, Lewis Shale	0.05	Dube <i>et al.</i> , 2000
Porosity, Fruitland Formation	0.09	NM Oil & Gas
Porosity, nuclear chimney	0.34	calibrated
Porosity, explosion-generated fractures	0.1	calibrated
Porosity, hydraulic fractured sandstone	0.1	best estimate
Capillary pressure, Pictured Cliffs	TRUST fit	Core Laboratories, 1971
Relative perm., PC, Lewis Shale, Fruitland Fm	van Genuchten	see text for parameters
Capillary pressure, Lewis Shale & Fruitland Fm	van Genuchten	see text for parameters
<sup>3</sup> H radioactivity, liquid and gas, Ci	40,000	Smith, 1970
Diffusion coeff., HTO in methane, $m^2 s^{-1}$	$2.92 \times 10^{-5}$	Cussler, 1997
Diffusion coeff., HTO in liquid water, $m^2 s^{-1}$	$3.47 \times 10^{-9}$	Mills, 1973
Diffusion coeff., CH <sub>4</sub> in liquid water, $m^2 s^{-1}$	$1.49 \times 10^{-9}$	Reid <i>et al.</i> , 1987
Tortuosity	const.	See text
<sup>3</sup> H half-life, yr	12.32	Lucas and Unterweger, 2000
<b>Initial Conditions</b>		
Parameter	Value	Source
Formation pressure at base, MPa	7.24	Ward and Lemon, 1968
Gas saturation	0.6	Ward and Lemon, 1968
Reservoir temp., °C	54	Ward and Lemon, 1968
Mass fraction tritium in aqueous phase	$4.6 \times 10^{-10}$	Calculated, see text

<sup>1</sup> New Mexico Energy, Minerals and Natural Resources Department, <http://www.emnrd.state.nm.us/>.

As implemented with the EOS7r equation of state module, TOUGH2 solves equations for two phases (gas and liquid [or aqueous]) and five components: water, methane (replaces air), brine (not considered), radionuclide 1 (tritiated water), and radionuclide 2 (helium, though it is not radioactive and is ignored). Radionuclide 2 is the decay component of radionuclide 1. The gas phase is composed of methane, water vapor, tritiated water vapor, and helium. The liquid phase is composed of water, tritiated water, dissolved methane, and dissolved helium. The governing equations are presented in Appendix A.

## 3.4.2 Rock properties

### 3.4.2.1 Intrinsic permeability

#### 3.4.2.1.1 Nuclear cavity and chimney

The chimney formed when enough heat from the nuclear detonation was released to cause vaporization of the surrounding rock. The chimney radius was calculated to be 25 m (80 ft) with a height of 101 m (333 ft) (Korver and Rawson, 1968) and assumed to be a porous medium of uniform permeability. The chimney was assumed to terminate at the interface between the Pictured Cliffs Sandstone and Fruitland Formation (Rawson *et al.*, 1968). Reentry drilling in GB-E (renamed GB-ER) terminated approximately 5 m below the top of the Pictured Cliffs, through a 3 m void, which was determined to be the top of the chimney. No data are available with respect to the porosity and permeability of the chimney, so these parameters were determined by calibrating pressure to a production test conducted between late June and November, 1968 (AEC, 1971). Details of the calibration are discussed below, but the best fit resulted in chimney intrinsic permeability of  $10^{-13}$  m<sup>2</sup> and porosity of 0.34.

It is important to realize that the chimney is a rubble-filled void with a puddle of solidified melt glass on the bottom and glass possibly covering part of the chimney walls. Much of the rubble is likely the size of boulders such that the concept of the chimney being a continuous, uniform porous medium is not strictly true. If this is the case, then modeling flow and transport through the chimney using continuum equations, such as Darcy's law, has a limitation. This limitation is overcome by recognizing that the details of the mixing of fluids in the chimney are not very important. Instead, the chimney is seen as a highly permeable source of uniformly mixed radionuclides that are able to migrate outward into the surrounding fractures and native formations.

#### 3.4.2.1.2 Nuclear-stimulated zone

The nuclear detonation released a shock wave that fractured rock radially outward from the detonation. A full three-dimensional picture of the fracture network and its spatial properties is not known, as it is affected by bedding, preexisting weaknesses of the rock, jointing, and presence of low-density coals (Rawson *et al.*, 1968). Porosity and caliper logs were run in GB-2 and GB-ER (a sidetracked hole) before and after the detonation and suggested that the porosity had "changed" (Rawson *et al.*, 1968), suggesting that the shock wave had resulted in fractures at that distance (GB-2 is 92 m from GB-ER). Porosity and caliper logs suggest that the fracture extent exceeded the preshot estimates of 120 m (395 ft) in the Pictured Cliffs and 150 m (490 ft) in the Lewis Shale, although it was not stated by how much the preshot estimates were exceeded (Rawson *et al.*, 1968). Because of this unknown, the model was set up such that the fracture zone in the Pictured Cliffs extends 120 m radially from the detonation and 150 m horizontally from the detonation in the Lewis Shale (Figure 7). It is assumed in the model that the distance pervades each formation vertically. Although it is possible that single fractures may have reached the estimated distances, it may not be reasonable to conclude that each formation was uniformly fractured vertically and radially. However, in the model the entire Pictured Cliffs Sandstone and upper part of the Lewis Shale are considered to be uniformly fractured by the nuclear detonation, which is consistent with an equivalent porous medium model of fractures.

No reliable estimates of permeability of the fractured rock associated with the nuclear detonation are found in the literature. In lieu of permeability estimates, fracture permeability was determined by calibrating the model to a 15-day production test, followed by 100 days of recovery. The manner in which the value for permeability,  $10^{-14} \text{ m}^2$ , was chosen is discussed below.

#### **3.4.2.1.3 Pictured Cliffs Sandstone**

The average intrinsic permeability of the Pictured Cliff Formation, based on air permeability measurements on cores from GB-1 and GB-2, is  $1.5 \times 10^{-16} \text{ m}^2$  (0.16 md). Analysis of flow tests performed on GB-2 estimated a permeability-thickness (sometimes known as a formation potential) as 1.7 to 3.0 md-ft (Ward and Lemon, 1968). The thickness of the formation tested is not given and if it is greater than 20 ft, then the permeability as determined from the flow tests is less than the mean  $1.5 \times 10^{-16} \text{ m}^2$  measured from the cores. As discussed below, the Pictured Cliffs Sandstone permeability and porosity were considered adjustable parameters in the calibration to the flow test done on GB-ER. The Pictured Cliffs permeability resulting in the best fit is  $10^{-16} \text{ m}^2$ .

#### **3.4.2.1.4 Fruitland Formation and Lewis Shale**

The Fruitland Formation is a low-permeability sandstone, siltstone, shale, and coal with a permeability estimated as  $10^{-17} \text{ m}^2$  (New Mexico Oil and Gas Database). This is based on cores from wells located primarily in Township 30 North, Range 6 West (the Gasbuggy site is located in T29N R4W).

Measurements on cores of intrinsic permeability of the Lewis Shale indicate that the mean matrix permeability is  $10^{-19} \text{ m}^2$  ( $10^{-4}$  md). The more important mean effective permeability of the reservoir, which includes fracture permeability, is  $1.5 \times 10^{-17} \text{ m}^2$  (Dube *et al.*, 2000), based on tests in the two nearby townships T28N R5W and T28N R4W (T28N R4W is directly south of T29N R4W).

#### **3.4.2.1.5 Hydraulic fracture zone**

The extent of the fracture pattern associated with hydraulic stimulation is rarely known a priori. Fractures have been thought to extend as far as 1,000 ft, but these cases seem rare, the connectivity is not known, and these instances are poorly documented. In the model, it was assumed that the fracture zone extended 150 m (500 ft) from the hypothetical gas production well along the principal direction of maximum stress and half that distance perpendicular.

There are no reliable relationships about fracture network permeability associated with hydraulically produced fractures. This is generally not known until the well is tested after the stimulation. With no other guidance, the intrinsic permeability of the hydraulic fractures surrounding the production well is conservatively estimated as 500 times the permeability of the native formation. In other words, the fracture permeability is  $5 \times 10^{-14} \text{ m}^2$  in the  $x$ - $z$  plane. It would be expected that the fracture apertures would be reduced further from the stimulation location so that there would be a corresponding reduction in permeability. To capture this behavior, the last 40 m of the fracture zone outward from the well, along the principal axis, was reduced to being 50 times the permeability of the native formation in  $x$ - $z$  plane ( $5 \times 10^{-15} \text{ m}^2$ ).

### 3.4.2.2 Porosity, saturation, capillary pressure, and relative permeability

#### 3.4.2.2.1 Porosity of the nuclear chimney

The porosity of the chimney is a calibration parameter (see below) and was estimated as 0.34. Simulations were run with a chimney porosity of 0.35 and 0.40, and the results were not found to be sensitive to the porosity.

#### 3.4.2.2.2 Porosity of all other rock types

A porosity of 0.10 is used for the Pictured Cliffs Sandstone (Ward and Lemon, 1968). This is the matrix porosity, but flow is likely controlled by fracture porosity, which is unknown but probably between 0.01 and 0.1. Based on air permeability measurements on cores, the porosity of the Fruitland Formation matrix is between 0.01 and 0.13 with the average value of 0.09 used in the simulations (ConocoPhillips verbal comm.). Porosity of the Lewis Shale is reported as 0.02 (ranging from 0.02 to 0.08; Dube *et al.*, 2000). One-dimensional simulations run to steady state revealed that the low porosity resulted in liquid water contents in excess of 0.9 in the shale, which seemed unreasonable. The porosity was raised to 0.05 (still within the range of measured values), which resulted in steady-state liquid water contents ~0.75, which is more characteristic of water contents in the region. Fracture porosity is usually unknown in geologic formations, but is assumed to be less than matrix porosity due to the sparse nature of the narrow fractures. However, due to the nature in which the nuclear-generated fractures were formed, a value of 0.10 was used in the model. The same value is used for the hydraulic fractures, because to some extent they will be held open by proppants injected with the hydraulic fracturing fluid.

#### 3.4.2.2.3 Phase saturation

Phase saturation is the ratio of fluid volume to pore volume for a given phase. Gas and water flow are assumed to be in a condition of dynamic steady state prior to the detonation, so in situ liquid saturation is assumed to closely represent residual liquid saturation. Each simulation was begun with  $S_l=0.6$  (Ward and Lemon, 1968).

#### 3.4.2.2.4 Capillary pressure

Capillary pressure measurements from six cores from the Picture Cliffs Sandstone are shown in Figure 8 (Core Laboratories, 1971). The TRUST function in the TOUGH2 computer program was fit to the data:

$$P_{cap} = -P_e - P_o \left[ \frac{1 - S_l}{S_l - S_{lr}} \right]^{1/\eta} \quad \text{for } S_{lr} < S_l < 1 \quad (1)$$

$$P_{cap} = 0 \quad \text{for } S_l = 1 \quad (2)$$

where  $P_o$  is a reference pressure (1700 Pa),  $S_l$  is the (variable) liquid saturation,  $S_{lr}$  is residual liquid saturation (0.4),  $\eta$  (=0.8) is a curve-fit parameter,  $P_e$  (=1.5 x 10<sup>3</sup> Pa) is a reference pressure, and the saturations are all volumetrically based. The van Genuchten (1980) function was used for capillary pressure of the Lewis Shale and Fruitland

Formation, using values typical for clay from Carsel and Parrish (1988). The maximum capillary pressure achievable in the chimney is 40 kPa, similar to the Rulison model (Cooper *et al.*, 2010), so that drainage is rapid and water high in the chimney quickly drains down and puddles at the bottom.

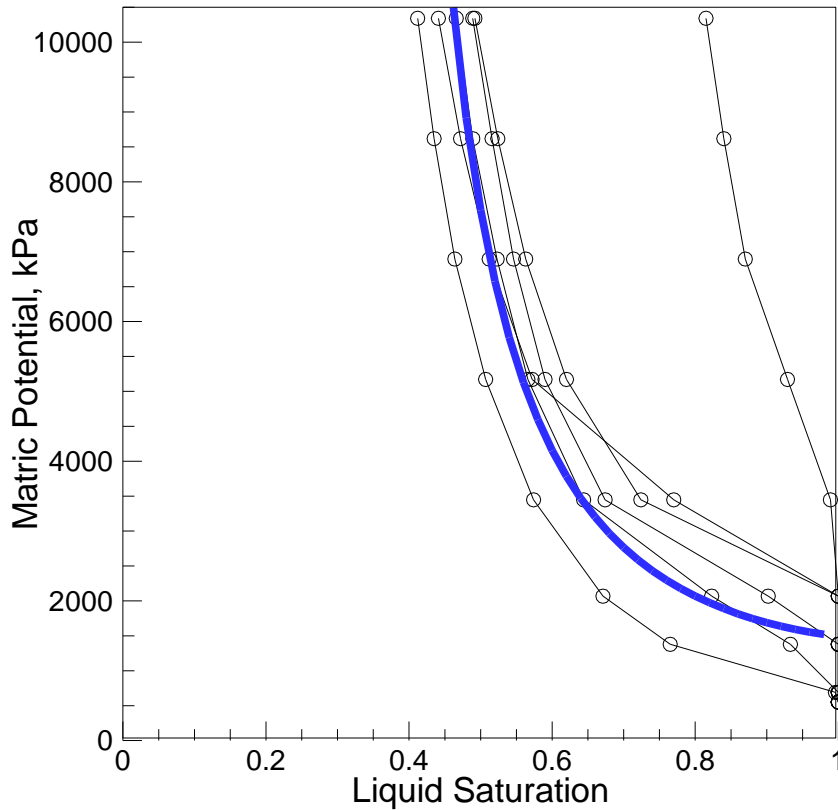


Figure 8. Capillary pressure curves from six cores (circles) from the Pictured Cliffs Sandstone and best fit (blue) through the majority of the data. Data for the core with high saturation values above 0.8 were ignored in the curve fit.

### 3.4.2.2.5 Relative permeability

Relative permeability of the Pictured Cliffs Sandstone is from measurements of permeability to gases measured by Thomas and Ward (1972) at three different confining pressures (Figure 9). The measurements made at 3,000 and 6,000 psi (20.7 and 41.3 MPa, respectively) confining pressures are very similar and a curve was fit through the data using the van Genuchten (1980) function (for water):

$$k_{rl} = \begin{cases} \sqrt{S^*} \left\{ 1 - \left( 1 - [S^*]^{1/m} \right)^m \right\}^2 & \text{for } S_l < S_{ls} \\ 1 & \text{for } S_l \geq S_{ls} \end{cases} \quad (3a,b)$$

where  $S^* = (S_l - S_{lr}) / (S_{ls} - S_{lr})$ . The relative permeability to gas is:

$$k_{rg} = \begin{cases} 1 - k_{rl} & \text{for } S_{gr} = 0 \\ (1 - \hat{S})^2 (1 - \hat{S}^2) & \text{for } S_{gr} > 0 \end{cases} \quad (4a,b)$$

where  $\hat{S} = (S_l - S_{lr}) / (1 - S_{lr} - S_{gr})$  and  $S_{gr}$  is the residual gas saturation. Equation (4b) is the Corey (1954) relative permeability curve to gas. Because the data were measured with gas and the function is for liquids, the assumption is made that the gas and liquid relative permeabilities sum to one for all saturation values. The curve for relative permeability to liquid was then developed by simultaneously fitting the gas data while adjusting the parameters. Throughout much of the domain, liquid water saturation is  $\sim 0.5$ , where relative permeability to water is greater than for gas. The highest water saturation achieved was around 0.65, meaning that significant entrapped air is present and it is extremely difficult for the rocks to become water-saturated under reservoir conditions. The same relative permeability functions used in the Rulison model (Cooper *et al.*, 2010) for nuclear-generated and hydraulic fractures and for the chimney (because it is essentially composed of slumped and fractured rock) were used here (Figure 10).

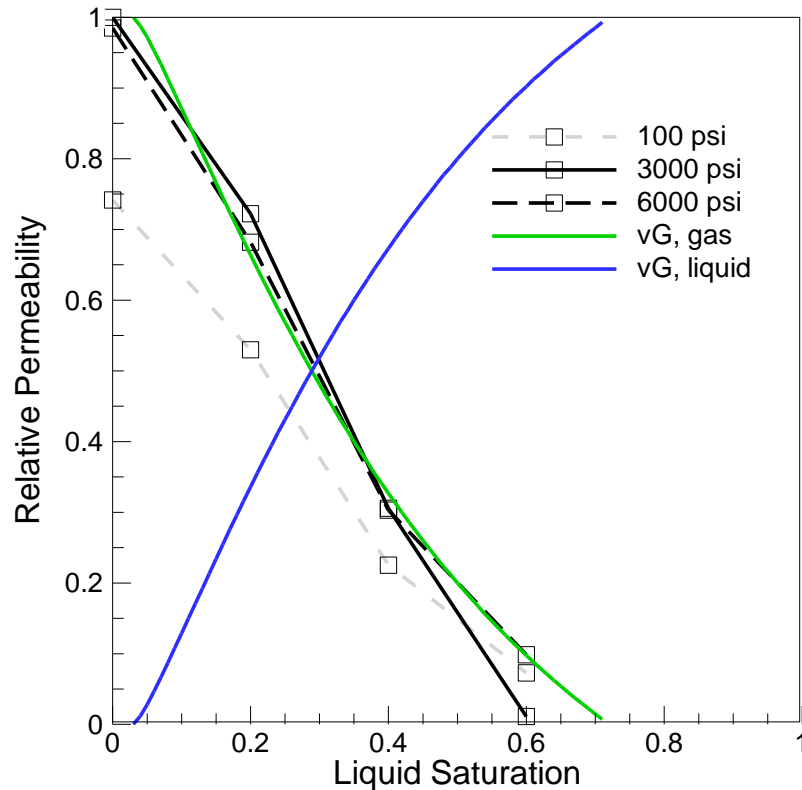


Figure 9. Data used for relative permeability (squares) to gas and the van Genuchten (1980) fit used for the model (green) for the Pictured Cliffs Sandstone. The blue curve is relative permeability to liquid water and was developed from the gas curve.

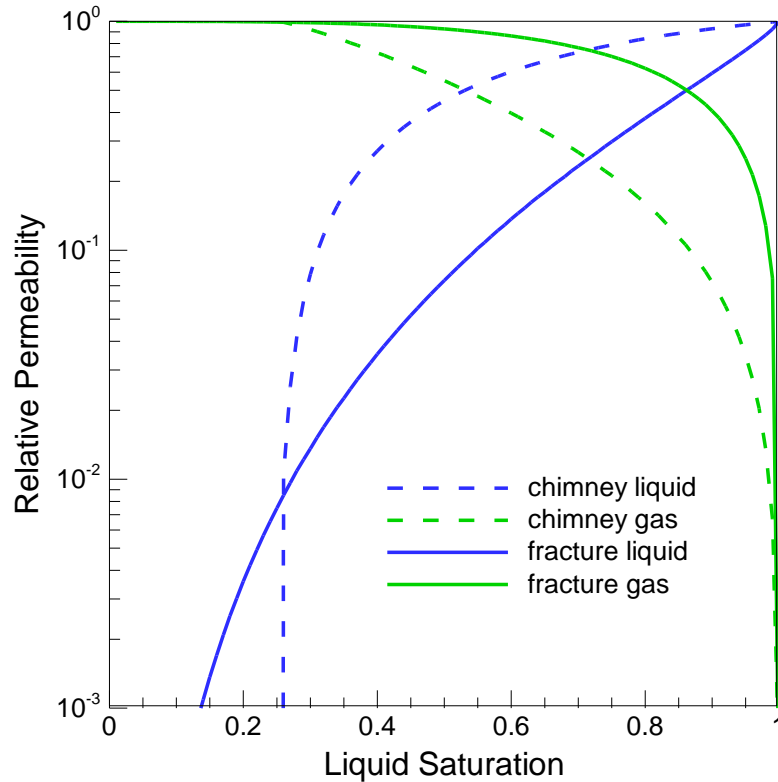


Figure 10. Relative permeability curves to gas (green) and liquid water (blue) for the nuclear chimney and detonation-induced fractures.

### 3.5 TRANSPORT MODEL PARAMETERS

#### 3.5.1 Chemical transport properties

The only transport constituent in the model is tritiated water ( $^1\text{H}^3\text{HO}$  or HTO). Other compounds that could have formed with tritium—such as the tritiated gases  $^3\text{H}$  (or T),  $^3\text{HH}$  (or TH), and methane compounds  $\text{CH}_3\text{T}$ ,  $\text{CH}_2\text{T}_2$ , etc.—are assumed to have either been removed during the first few years of testing that followed the detonation or never formed at all.

The following diffusion coefficients for gas mixtures are required: tritiated water and helium (the nonradioactive decay product of tritium) in methane. The free-air diffusion coefficient for tritiated water in methane was calculated using the method of Chapman and Cowling (see Reid *et al.*, 1987). The effect of pressure on diffusivity (Reid *et al.*, 1987, Equation 11-5.1) was investigated by Cooper *et al.* (2007) for the Rulison model and its effect was found to be negligible at those reservoir pressures (20 MPa at Rulison vs. 7.2 MPa at Gasbuggy). The free-air diffusion coefficient for helium has been measured and is reported in Cussler (1997). In the aqueous phase, molecular diffusion coefficients are required for HTO and He in water. Again, measured values of helium at infinite dilution are provided in Cussler (1997) and tritiated water in liquid water was determined using the method of Wilke and Chang, which accounts for reservoir pressure (see Reid *et al.*, 1987).

The free-air (for gases) and molecular (for liquids) diffusion coefficients are multiplied by a tortuosity factor to account for the complicated paths in the porous medium and fractures that effectively lengthen the travel path. As defined in TOUGH2, tortuosity can be considered as having a porous medium-dependent part,  $\tau_o$ , and a saturation-dependent part,  $\tau_\beta$ . The Millington-Quirk tortuosity model (Millington, 1959; Millington and Quirk, 1961; Jury *et al.*, 1991), which incorporates phase-dependent saturation, was implemented in the simulations. That is:

$$\tau_o \tau_\beta = \phi^{1/3} S_\beta^{10/3} \quad (5)$$

where  $\phi$  is porosity and  $S_\beta$  is the phase saturation. Because gas flow is assumed to occur primarily through fractures, Equation 5 was made constant so that it would not vary with gas saturation, which was assumed to always be close to unity (Cooper *et al.*, 2009). The tortuosity constants were developed for a porosity of 0.1 and gas phase saturation 0.4 ( $S_l = 0.6$  for the aqueous phase). The resulting tortuosity values are 0.0219 for the gas phase and 0.0846 for the aqueous phase. These values are multiplied by the infinite-dilution diffusion coefficients in Table 1 to obtain the true diffusion coefficients used in the model.

### 3.6 RADIOACTIVE SOURCE VALUES

As discussed in section 1.3 “Radionuclides of Potential Concern,” the total amount of tritium radioactivity released from the detonation was estimated as  $40,000 \pm 5,000$  Ci (Tewes, 1979). At present day, due to decay, there are approximately  $2,830 \pm 354$  Ci of tritium in the subsurface. All tritium is assumed to exist in the gas and liquid phases (i.e., none is assumed to be embedded in the melt glass). The tritium source is initiated in the model as mass fraction in the aqueous phase, which partitions thermodynamically (based on Henry’s law) into the gas phase during the first time step. Mass fraction of tritium in a given phase is the ratio of tritium mass in the phase to the total mass of the phase. To determine the initial mass fraction, the 40,000 Ci of tritium were converted into mass ( $1 \text{ Ci T} = 6.906 \times 10^{-7} \text{ kg HTO}$  [Cooper *et al.*, 2007]) and divided by the amount of water in the chimney. The amount of water in the chimney was determined from the results of the steady-state simulation, which was run to establish the initial pressure and liquid saturation conditions for the tritium transport calculations. The mass fraction of tritiated water in the aqueous phase ( $X_l^{HTO}$ ; mass of tritiated water in the aqueous phase per unit mass of liquid water) is  $4.6 \times 10^{-10}$ .

### 3.7 TRANSIENT PARAMETERS

#### 3.7.1 Gas well production characteristics

In addition to estimating the distance that radionuclides have traveled to the present day, simulations were run to determine the minimum distance a hypothetical gas production well could be located and not intercept radionuclides over its (assumed) 30-year production life. The production interval is located in the center of the Pictured Cliffs Sandstone, at the same elevation as the center of the chimney, but located 40 m above the working point (located in the Lewis Shale). The well is assumed to operate on deliverability against a well head pressure of 5.5 MPa (800 psi). No allowances were made for pressure drop in the well. Gas production is modeled as:

$$q_{\beta} = \frac{k_{r\beta}}{\mu_{\beta}} \rho_{\beta} \cdot \text{PI} \cdot (P_{\beta} - P_{wb}) \quad (6)$$

where  $q_{\beta}$  is the flow rate of a phase (gas, in this case,  $\text{L}^3 \text{t}^{-1}$ ),  $k_{r\beta}$  is the relative permeability to the phase [ $\text{L}^2$ ],  $\mu_{\beta}$  is the dynamic viscosity of the phase [ $\text{M L}^{-1} \text{t}^{-1}$ ],  $\rho_{\beta}$  is fluid density of the phase [ $\text{M L}^{-3}$ ],  $P_{\beta}$  is the phase pressure in the reservoir [ $\text{M L}^{-1} \text{t}^{-2}$ ], and  $P_{wb}$  is the phase pressure at the wellbore. The productivity index (PI) is a factor that accounts for the fact that the wellbore does not consist of the entire (i.e., much larger) grid block and is defined as:

$$(\text{PI})_l = \frac{2\pi(k\Delta z_l)}{\ln(r_e/r_w) + s - \frac{1}{2}} \quad (7)$$

where  $k$  is the intrinsic permeability ( $\text{m}^2$ ),  $\Delta z_l$  is the thickness of the production zone (10 m),  $r_e$  and  $r_w$  are the radii of the grid block and (effective) well, respectively, and  $s$  is a skin factor (Horne, 1995). The skin is a damaged zone around the well that is invaded by mud filtrate or cement during drilling and well completion, causing a reduction in permeability and a greater drop in pressure at the well. The skin factor was assumed to be zero, meaning that there is no decrease in permeability around the well due to filtrate. The gas well simulated is typical of wells in the area, where production in the third year is 18.75 MMCF, which drops to around 12 MMCF for the remaining years (Figure 11). The simulation produced gas for the first 13 years in accordance with higher producing wells in the area, although after 15 years the simulation clearly overproduced gas by a factor of two. The reason is probably that the drainage radius of the actual production tests may have encountered rocks with permeabilities different than those used in the model. The PI in the simulation is  $1.4 \times 10^{-13}$ .

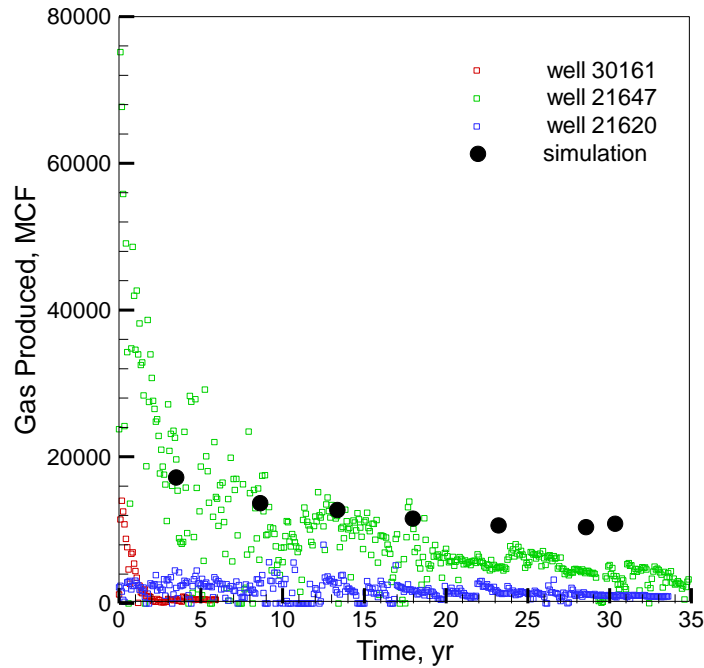


Figure 11. Gas produced, in thousand cubic feet, for three wells (colors) and the simulation (black circles).

### 3.7.2 Hydraulic fracture zone geometry

Despite the interest in hydraulic fracturing in recent years, understanding of fractures—their development, density, hydraulic properties, degree of connectedness, and behavior of fluid flow through them—is largely embryonic. There are no accurate models to predict the extent and subsequent hydraulic properties of a block of rock on the scale of tens of meters subject to hydraulic fracturing. Much of what is known is drawn from scaling laboratory-scale experiments to field scale and by inverse modeling of flow around wells that have already been fractured. This dovetails with the decades-old problem of not being able to use continuum models based on finite-difference and finite-element methods to make reasonable predictions of flow through even a single fracture. Despite these limitations, it is understood that hydraulic fracturing enhances permeability in the vicinity of the well and favors the direction of maximum principal stress. Fractures are modeled as an equivalent porous medium (EPM), as opposed to being implemented individually in the domain. The length of the fracture zone is assumed to be 150 m (500 ft) in the Pictured Cliffs, based on conversations with operators in the area. The length of the zone in the  $y$ -direction (least principal stress) is assumed to be 75 m. This results in a hydraulically fractured “zone” that is 300 m in the  $x$ -direction, 150 m in the  $y$ -direction, and 100 m in the  $z$ -direction (the entire Pictured Cliffs Sandstone is assumed to be fractured).

### 3.8 PARTIAL MODEL CALIBRATION TO NUCLEAR CHIMNEY

The initial cavity caused by the detonation was estimated to have a radius of 25 m. Within a day of the test, the roof of the cavity collapsed, resulting in a chimney filled with rubble. To determine the permeability of the chimney and surrounding fractures, the model was calibrated to a 15-day production test that was followed by 100 days of recovery (AEC, 1971). After some initial testing in January 1968, the well was shut until June 28, 1968. The initial shut-in bottom-hole pressure (BHP) at a depth of 1,155 m (3,790 ft) was 6.55 MPa (950 psi) on January 17, 1968, and rose to 7.35 MPa (1,067 psi) on June 28, 1968. The well was then flowed at 5 MMCFD for six days, at which time the BHP dropped to 906 psi, and was then shut in for 24 hours. Testing resumed for five days at 5 MMCFD, and flow was then lowered to 750 MCFD for four days. The well was then shut in until November 4, 1968, at which time another production test was begun. A total of 57 MMCF of gas was produced during the 16 day production period (AEC, 1971).

Calibration was done by first running the model to steady-state natural conditions for  $10^5$  years, adding the chimney and nuclear-generated fractures and calibrating to the flow test. Neither the chimney geometry nor the nuclear-generated fracture extent were adjusted during the calibration. Only the intrinsic permeability of both and the chimney porosity were varied between simulations to fit the data. The result is shown in Figure 12. The properties that fit the production curve best are  $k_{\text{chim}}=10^{-12}$  m<sup>2</sup>,  $k_{\text{nuke frac}} 10^{-13}$  m<sup>2</sup>, and chimney porosity 0.34. The nuclear-generated fracture porosity was determined a priori as 0.10. Some curves fit the early time better at the expense of late time behavior. Because no curves fit both the early time and late time well, it was decided to choose a curve whose properties fit the late time better, as this is assumed to more closely approximate the formation properties of the Pictured Cliffs. The properties of the chimney and explosion-generated fractures are seen as being less important because their properties will only affect the distribution of tritium within the chimney and fractures and have less effect on transport away from the detonation.

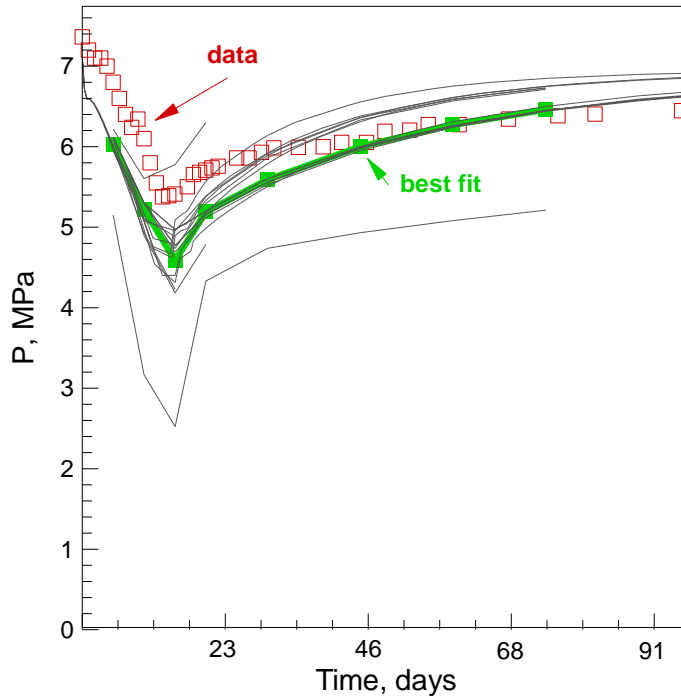


Figure 12. Bottom hole pressure as a function of time (red squares) from the 15-day production test in 1968 and subsequent recovery over the following four months. The best-fit curve (green line) is the pressure at the same elevation as the actual test with the same porosity and permeability as the chimney. The dark lines are other calibration attempts with different combinations of chimney permeability varying between  $10^{-14} \text{ m}^2$  and  $10^{-11} \text{ m}^2$ , and nuclear-generated fracture permeability between  $10^{-15} \text{ m}^2$  and  $5 \times 10^{-13} \text{ m}^2$ .

#### 4.0 MODEL RESULTS

The first step in the modeling sequence was to run a simulation without tritium to steady state in order to establish a dynamic steady state between gravity, pressure, and capillary forces throughout the solution domain. This steady state simulation is considered to approximate reservoir conditions prior to the Gasbuggy test. At the conclusion of the steady-state simulation, the resulting pressure and liquid saturation fields (i.e.,  $P$  and  $S_l$  at each grid block) were used as the initial condition for a 47-year tritium transport simulation, from late 1967 to present day. The rock conditions were changed—their permeability, porosity, capillary pressure, and relative permeability functions—for the grid blocks that would now become the chimney and surrounding nuclear-generated fractures. The model was restarted to simulate tritium transport for the 47-year period. Figure 6 shows the initial conditions in 1968. Although gas production testing of GB-ER occurred through November 1969, the gas production tests were not included in the model in order to maximize transport away from the chimney. If included, production testing would act to confine radionuclides to the chimney and nearby fractures and limit their diffusion away from it during the testing period. Although gas production during testing was not modeled, tritium removed from the subsurface during production testing was accounted for in the tritium balance, as discussed in sections 1.3 and 3.6.

The total pressure at the bottom of the chimney increased due to drainage of water through the (now) highly permeable rocks comprising the chimney and its ponding at the base. This created a slight outward pressure gradient, which, along with gas-phase diffusion, contributed to tritium migration away from the chimney in all directions. Figure 13 shows tritium concentration (as mass fraction of tritiated water) in the gas phase ( $X_g^{HTO}$ ) at the start of the 47-year period. Aqueous-phase tritiated water is uniformly applied to all chimney grid blocks at  $X_l^{HTO} = 4.6 \times 10^{-10}$  and partitioned after the first time step (1 second) into the aqueous and gas phases. As dictated by Henry's law, the bulk of tritium stays in the aqueous phase such that the mass fraction in the aqueous phase is essentially unchanged while a small amount partitions into the much less-dense gas phase (initial  $X_g^{HTO} = 7.6 \times 10^{-12}$ ).

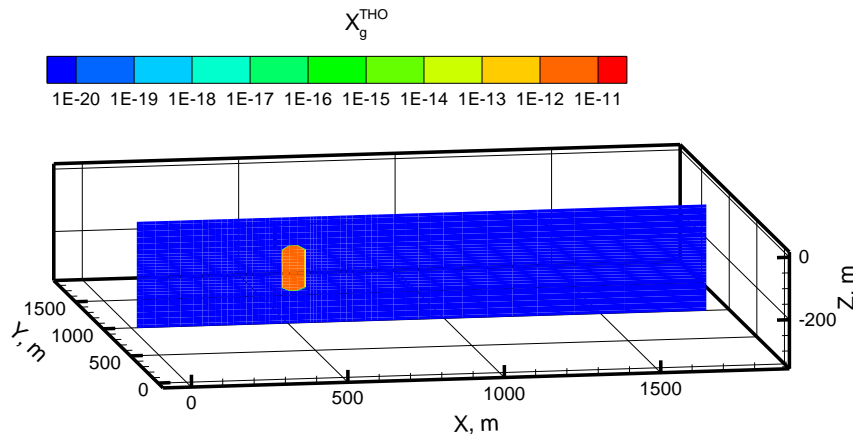


Figure 13. Initial mass fraction of tritium in the **gas** phase ( $X_g^{HTO}$  or tritiated water vapor) in December 1967 at the start of the simulation. This and subsequent figures display a two-dimensional slice through the three-dimensional model domain. The colors represent tritium concentration in the gas phase, as mass fraction. The color bar above the figure describes the mass fraction values from background (blue) to higher concentration in the warmer colors.

By 1993 (26 years after the detonation), tritium has spread as far as 110 m from the detonation point in the upper part of the Lewis Shale (Figure 14). The moisture contents in the Lewis Shale are as high as 0.86 (compared with 0.40 through most of the overlying Pictured Cliffs), suggesting that the heavily saturated aqueous phase would act to retard gas diffusion. By 2014 (Figure 15), diffusion in both phases has slowed to a point where it is balanced by radioactive decay. The leading edge of the tritium is still at 110 m, so it appears that tritium has stopped diffusing (although it actually has not) and that the tritium mass fraction is diminishing solely by radioactive decay. The shape of the HTO field in the gas phase at 26 and 47 years is similar (compare Figures 14 and 15), but the HTO mass fraction in the gas phase has substantially decreased in the center of the plume (by two orders of magnitude). Figure 16 shows tritiated water in the aqueous phase in the year 2014. The image appears to be identical to tritiated water in the gas phase (Figure 15) because both mass fractions are scaled to their maximum starting value. The reason that the tritium extent is matched in the two phases is that tritium travels in the higher diffusivity and permeability gas phase, but continually dissolves into the aqueous phase (thermodynamically, not kinetically) where it is able to achieve a mass fraction several orders of magnitude greater than the gas phase.

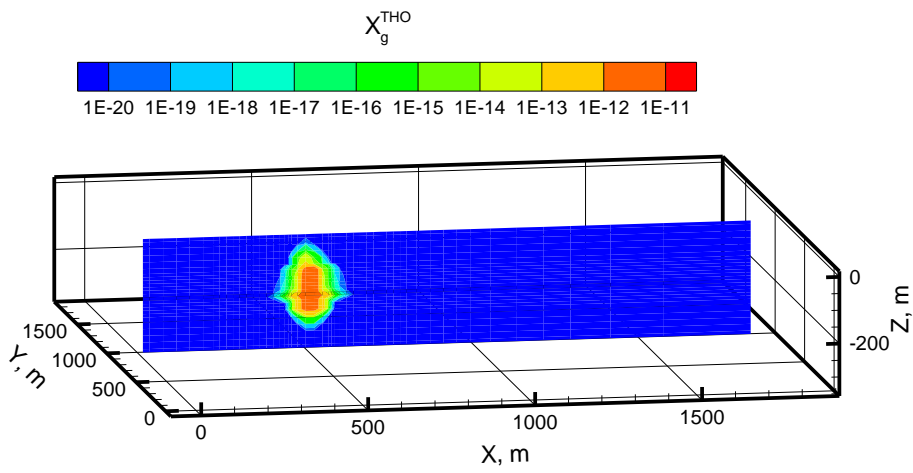


Figure 14. Mass fraction of tritiated water vapor in 1993, 26 years after the detonation.

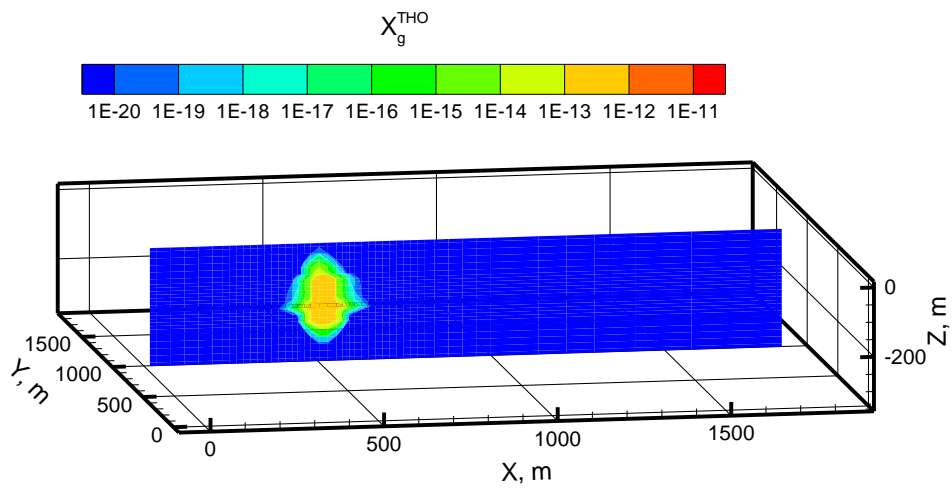


Figure 15. Mass fraction of tritiated water vapor in 2014, 47 years after the detonation.

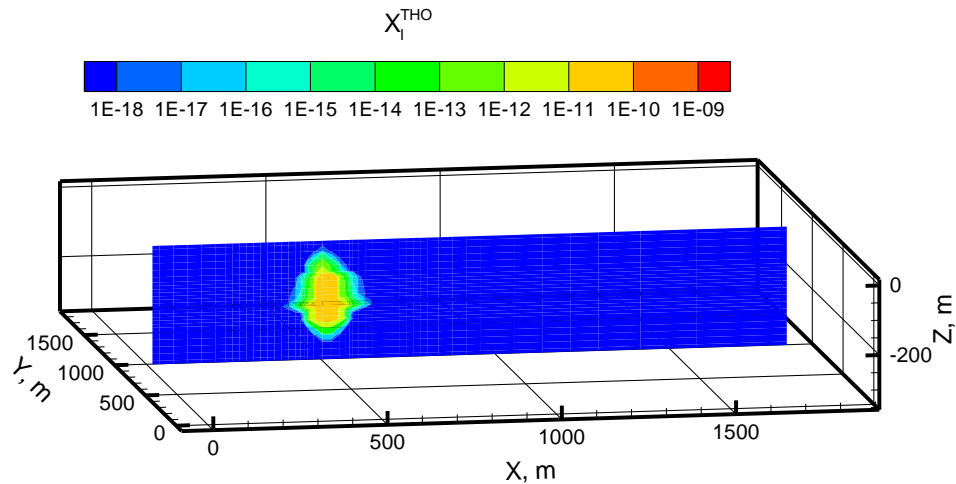


Figure 16. Mass fraction of tritiated **liquid** water in 2014, 47 years after the detonation. The pattern matches the  $X_g^{HTO}$  for the same time period because the each is scaled to its initial, maximum mass fraction.

#### 4.2 TRITIUM MIGRATION DURING GAS PRODUCTION

The model of unstressed (i.e., no gas production from wells) conditions was run for 47 years to present day, at which time the simulation was stopped and a producing gas well was added to the domain. The well is located 340-m distant along the principal axis, producing from a 10-m interval located in the middle of the Pictured Cliffs Sandstone. The choice of well location was guided by the desire to find the minimum distance that a well could be placed from the working point and produce gas for 30 years without capturing tritium from the detonation. This determination was done by running multiple simulations with the well in different locations and identifying the simulation that came closest to meeting the criteria. The well was assumed to operate on deliverability against a 2.75 MPa (400 psi) wellhead pressure with a PI (Equation 7) of  $1.4 \times 10^{-13}$ . Figure 17 shows the pressure field (contour lines) and tritiated vapor mass fraction field (contour colors) after three years of production. As expected, the pressure field extends to the chimney, but even though the gas velocities in the vicinity of the well are on the order of several meters per day, 50 m from the well they are approximately  $20 \text{ cm day}^{-1}$  and near the leading edge of the tritium “plume” they are only about  $2 \text{ cm day}^{-1}$ . The mass fraction field of tritiated water vapor eight years after the start of production (year 2022) shows the definite influence that gas production has on the flow of tritium through the Pictured Cliffs, but almost no effect on flow through the unfractured Lewis Shale is observed (Figure 18). At this time, the leading edge of the tritium plume has migrated 130 m from the working point and the mass fraction of HTO in the gas phase at the leading edge is  $X_g^{HTO} = 3 \times 10^{-18}$ . Figure 19 shows that after 18 years of gas production, the leading edge of the tritium has traveled 150 m from the detonation with  $X_g^{HTO} = 8 \times 10^{-19}$ . After 28 years of production (Figure 20), the leading edge of the tritium has reached 210 m from the detonation, with  $X_g^{HTO} = 4 \times 10^{-19}$ . After 30 years of production (year 2044), the leading edge of the plume is 230 m from the detonation and 90 m from the gas well (Figure 21). No tritium has reached the well at that time.

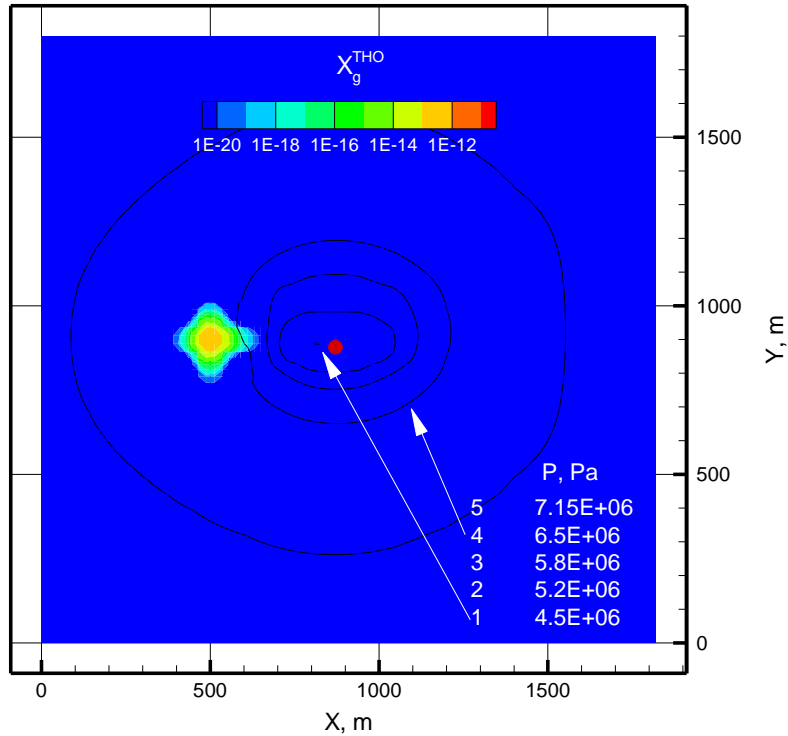


Figure 17. Map view of mass fraction of tritiated water vapor (color flood) and pressure (black contours) after three years of production. The drainage area (pressure field) clearly reaches the chimney, but the gas velocities are small enough that tritium does not reach the well. The hypothetical gas well is the red dot in the center of the figure. Because 6,891 Pa is equal to 1 psi, the equivalent pressure contours in pounds per square inch are 1040 (=  $7.15 \times 10^6$  Pa), 943, 842, 755, and 653 (=  $4.5 \times 10^6$  Pa) psi.

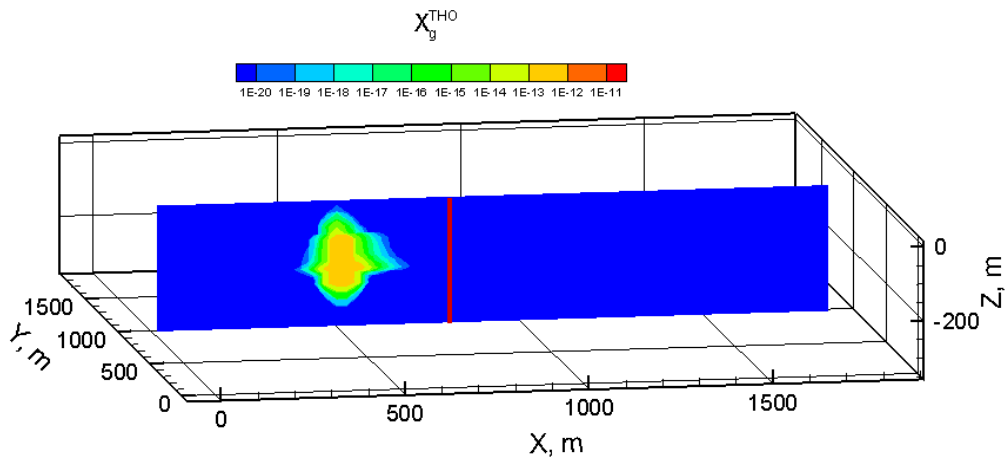


Figure 18. Mass fraction of tritiated water vapor in 2022, 55 years after the detonation and 8 years after the start of gas production from a hypothetical well (red vertical line) located 340 m from the detonation. Gas production is from a 10-m interval located at the center of the Pictured Cliffs Sandstone.

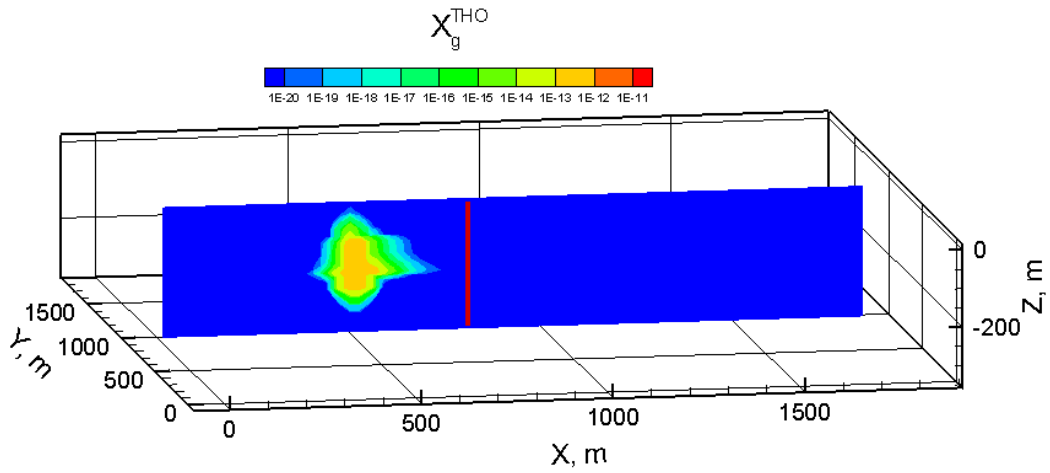


Figure 19. Mass fraction of tritiated water vapor after 18 years of gas production, in the year 2032.

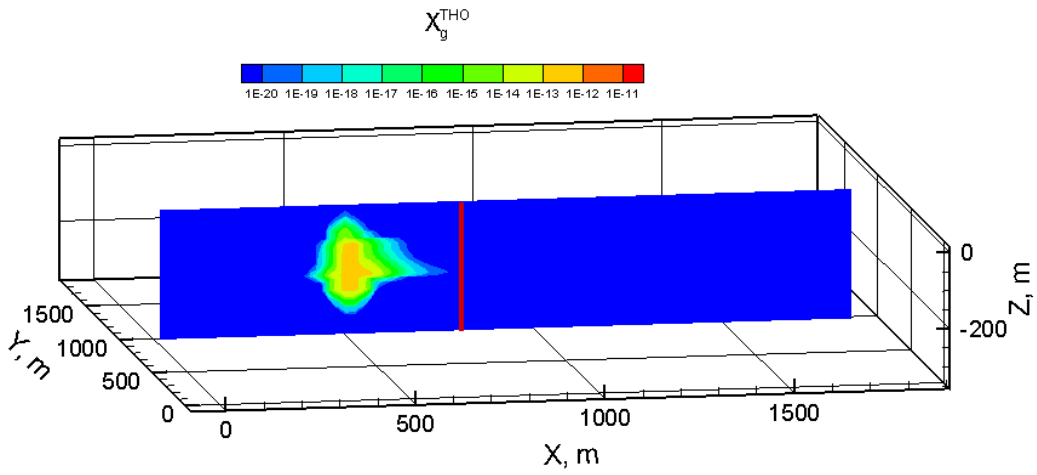


Figure 20. Mass fraction of tritiated water vapor after 28 years of gas production, in the year 2042.

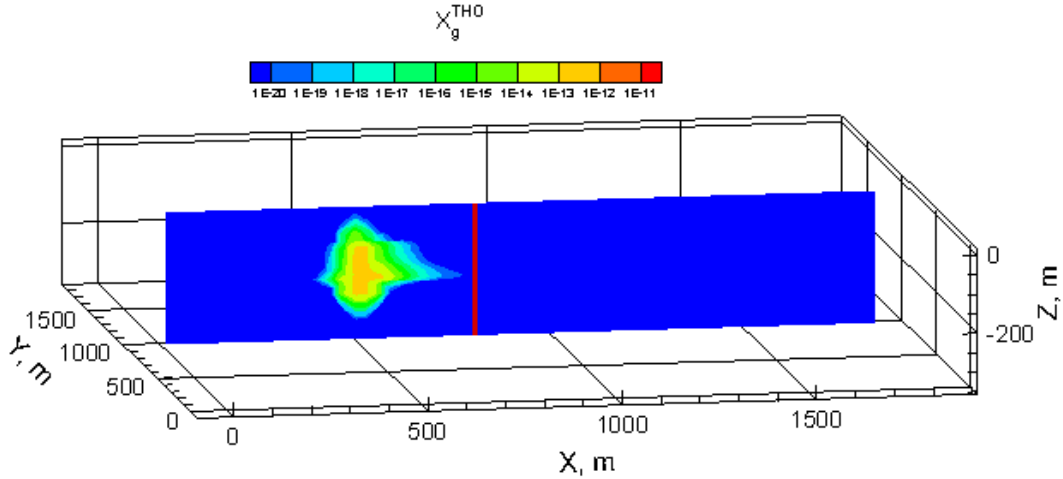


Figure 21. Mass fraction of tritiated water vapor after 30 years of gas production, in the year 2044.

After 30 years of gas production, the mass fraction of tritium in the aqueous phase,  $X_l^{HTO}$ , at the leading edge of the plume is  $2 \times 10^{-18}$ . Gas flows to the well radially (i.e., in all directions with equal velocities). Tritium above background never reaches the well not only because the gas velocities are small, but also because gas from other directions mixes with gas migrating from the vicinity of the chimney. Additionally, the 12.32-year half-life of tritium means that 3.8 half-lives have passed since the detonation through the year 2014. At the end of production, a total of 2.3 BCF (billion cubic feet) of gas is produced with 2.67 million barrels of water. Gas production lasted for 30 years, at that time (year 2044), production was stopped and the drainage field was allowed to recover. Figure 22 shows that 120 years after the detonation (year 2087, 43 years after gas production stopped), HTO is still present in the reservoir but its maximum mass fraction in the gas phase has decreased to  $\sim 10^{-14}$  and the leading edge has retreated from the well. The leading edge of the HTO plume is 150 m from the former gas well.

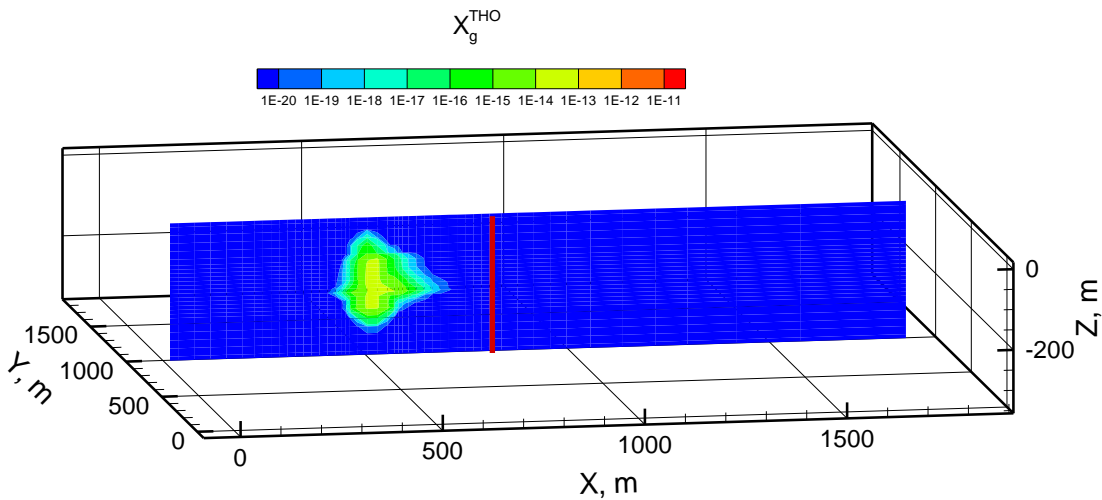


Figure 22. Mass fraction of tritiated water vapor 120 years after the detonation, in the year 2087, 43 years after gas production has ceased.

A simulation was run in which the well was moved 400 m from the working point and the deliverability pressure was raised to 5.5 MPa (800 psi). The PI was also raised to account for a skin value of 10 (Equation 7). Figure 23 shows that the drainage radius encloses the chimney, but has little effect on the tritium distribution, as the leading edge has extended only an additional 10–20 m beyond its location at the end of 47 years.

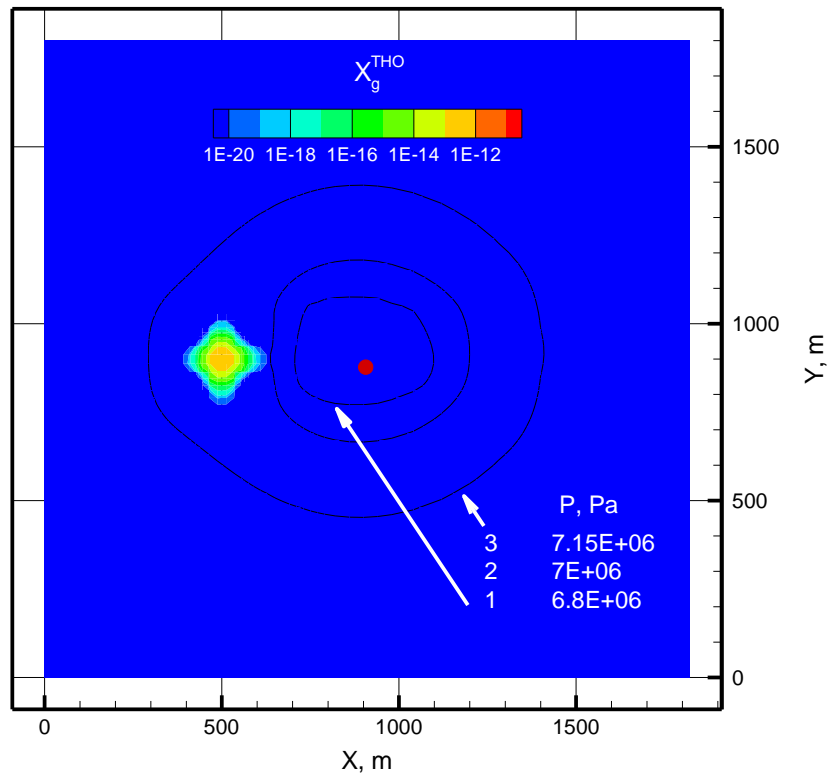


Figure 23. Map view of mass fraction of tritiated water vapor (color flood) and pressure (black contours) after three years of production for a deliverability pressure of 800 psi (5.5 MPa) from a well located 400 m from the working point. The hypothetical gas well is the red dot in the center of the figure. The contours in pounds per square inch are 1,040, 1,020, and 987 psi.

## 5.0 CONCLUSIONS

The overarching objective of this project is to develop a model that can be used to support strategic planning for long-term surveillance and maintenance of the Gasbuggy site. Two specific objectives are as follows:

1. *Estimate the extent of radionuclide contamination in the subsurface at the present day.*

The present day extent of tritium migration (as tritiated water [HTO]) from the nuclear detonation is expected to be approximately 110 m from the working point with most of this transport through the chimney and surrounding rock fractured by the detonation. The main

transport process is diffusion in the gas phase. Aqueous phase diffusion (i.e., through liquid water) also occurs but is a much slower process—typically four orders of magnitude slower owing to the difference in diffusion coefficients for HTO in gases and liquids. However, diffusion in each phase is not an isolated process. The phases are coupled by the ability of HTO to transfer from the gas phase into the aqueous phase in a proportion such that at any time over 100 times more tritiated water exists in the aqueous phase as in the gas phase. The important point is that although tritium *migrates* primarily as gas HTO, it is primarily *stored* as liquid water. Tritium migration is primarily a function of porosity and tortuosity. Because its migration is primarily driven by diffusion, permeability has almost no role in transport. Because the tortuosity of fractures is unknown, the conservative approach was taken that they are fairly straight, resulting in faster (and further) migration than would occur through more tortuous pores in the rocks. Other gaseous radionuclides of potential concern,  $^{14}\text{C}$  and  $^{85}\text{Kr}$ , were largely removed from the chimney during production tests that followed the detonation. Nongaseous radionuclides are relatively immobile due to formation properties (low permeability to liquid) and transport properties (for example, sorption and presence in glass solids) and, as a result, are confined to the nuclear chimney.

2. *Forecast radionuclide migration during possible future production of natural gas from nearby wells.*

A scenario in which a hypothetical production well was assumed to produce gas for 30 years from a ten-meter interval in the middle (vertically) of the Pictured Cliffs Sandstone investigated the impact of production on tritium migration. A gas well located 340 m from the working point was placed in the domain. Gas was produced on deliverability at a pressure of 400 psi (2.75 MPa) from an assumed hydraulically fractured region with a permeability greater than the native permeability. The drainage radius reached the chimney within three years of gas production and clearly induced tritium migration toward the well, though tritium did not ever reach it. The HTO above background concentration came to within 90 m of the well, but the low permeability to gas, low pressure gradient, radioactive decay, and dilution with gas not contaminated with HTO all resulted in no HTO above background reaching the well. The well was located directly in line with the principal direction of the hydraulic fractures. Wells located off of this trend could theoretically be located closer to the chimney without inducing significant transport because the permeabilities would be lower when not aligned with the principal stress direction. The model domain is referenced only to the location of the nuclear chimney and can be oriented in any direction such that the  $x$ -direction (left-right in the figures) can be viewed as being in any of the possible directions of maximum principal stress where fracturing is expected to be greatest (N35E, N55W, or NS). The hypothetical production well is located 340 m from the working point and assumed to produce methane from a 10-m interval at the same subsurface elevation as the device working point. The 340 m distance was chosen through trial and error to induce migration because we cannot predict where an operator might drill or what intervals would be completed. The combination of distance to the gas well, the properties of the hydraulic fracture zone, the properties of the Pictured Cliffs Sandstone, and the gas production rate all work together to prevent tritium from reaching the well in the simulation.

The DOE controls the subsurface mineral rights to a depth of 152 m (500 ft) below the base of the Pictured Cliffs in the SW quarter of Section 36, T29N, R4W. The shortest distance from the Gasbuggy emplacement well to that boundary is approximately 244 m (800 ft) to the east. The well is not centered in the quarter section, so the distance is longer in other directions.

Based on the simulation of tritium diffusion since the nuclear test, tritium from Gasbuggy is currently contained within the DOE-controlled quarter section. Forecasting migration that could be affected by future nearby oil and gas extraction activities is subject not only to the uncertainties of the modeling process, but also uncertainty in what activities will take place and when. For the simulated conditions of a well 340 m from the nuclear test, beginning production now, tritium could migrate close to the boundary of the controlled quarter section after 30 years of production (specifically, within 10 meters in the shortest eastward direction, though that is not aligned with the direction of maximum principal stress). This suggests that stewardship of the Gasbuggy site will require vigilance to ensure that tritium is not removed from the quarter section by nearby oil and gas extraction activities. It is important to note that tritium migration is defined here as a mass-fraction concentration above background and does not necessarily represent a level that could present a risk to health or the environment.

Although the analysis presented here suggests that a production well can be located at a distance of 340 m or greater without causing migration of tritium beyond the control area, there are uncertainties in that estimate that are important to take into account. Many of these uncertainties were addressed in the model by using conservative assumptions that have the effect of allowing more tritium transport than is likely to occur, but the importance of other uncertainties is not clear. Any numerical model of flow and transport processes in the subsurface has inherent uncertainty due to the inability to observe and measure the spatially varying formation and fluid properties. Simulating fracture flow processes using an equivalent porous medium approach adds to this problem, as does neglecting second-order processes such as the test-derived heat, although this was shown to have a negligible effect on tritium transport for large distances and for times greater than one year (Cooper *et al.*, 2007). There are additional uncertainties regarding the distribution of fractures and radionuclides from the Gasbuggy test and the effect of production testing conducted from the nuclear chimney. There are also obvious uncertainties regarding where a future production well may be located with respect to the Gasbuggy test and the principal stress direction, how it will be completed (particularly relative to the detonation elevation), how it will be stimulated (e.g., hydrofracturing), how production will occur, and whether or not there are additional wells in production nearby. The timing of future production is important to an impact analysis because tritium continues to be removed by radioactive decay, so production wells drilled later in time will encounter lower tritium concentrations. These uncertainties in parameters and processes translate into an uncertainty in the tritium transport distance for the production scenario that should be remembered when considering the model results for stewardship decisions.

## 6.0 REFERENCES

- AEC (U.S. Atomic Energy Commission), 1971. Project Gasbuggy Manager's Report. Nevada Operations Office report NVO-37, p. 110.
- Borg, I.Y., R. Stone, H.B. Levy, and L.D. Ramspott, 1976. Information Pertinent to the Migration of Radionuclides in Ground Water at the Nevada Test Site Part 1: Review and Analysis of Existing Information. UCRL-52078 pt.1, Lawrence Livermore National Laboratories, p. 216.
- Burger, L.L., 1979. Distribution and reactions of tritiated hydrogen and methane. *In*, International Atomic Energy Agency, Behavior of tritium in the environment, Proceedings Series, Vienna IAEA-SM-232/54, STI/PUB/498, pp. 47-64.
- Carsel, R.F., and R.S. Parrish, 1988. Developing joint probability distribution of soil water retention characteristics. *Water Resources Research*, 24(5):755-769.
- Cooper, C., M. Ye, and J. Chapman, 2007. Tritium Transport at the Rulison Site, a Nuclear-Stimulated Low-Permeability Natural Gas Reservoir. DOE Office of Legacy Management Report DOE-LM/1521 2007, DOE Nevada Operations Office Report DOE/NV/13609-54. Desert Research Institute Publication No. 45224.
- Cooper, C., M. Ye, J. Chapman, and R. Hodges, 2009. Addendum: Tritium Transport at the Rulison Site, a Nuclear-Stimulated Low-Permeability Natural Gas Reservoir. Letter report from the Desert Research Institute to S.M. Stoller Corporation, Office of Legacy Management, U.S. Department of Energy, Grand Junction, Colorado.
- Cooper, C., J. Chapman, Y. Zhang, R. Hodges, and M. Ye, 2010. Update of Tritium Transport Calculations for the Rulison Site: Report of Activities and Results During 2009–2010. Letter report from the Desert Research Institute to S.M. Stoller Corporation, Office of Legacy Management, U.S. Department of Energy, Grand Junction, Colorado.
- Core Laboratories, Inc., 1971. Letter report to Mr. R.F. Lemon from Mr. Dare K. Keelan pertaining to Special Core Analysis Study Gas Buggy No. 1 Well, February 2, 1971, p. 29.
- Corey, A.T., 1954. The interrelation between gas and oil relative permeabilities. *Producer's Monthly*, vol. XLX, no. 1, November, pp. 38-44.
- DOE (U.S. Department of Energy), 2000. United States Nuclear Tests, July 1945 through September 1992, Nevada Operations Report DOE/NV-209-REV-15.
- DOE (U.S. Department of Energy), 2002. Site Characterization Work Plan for Gasbuggy, New Mexico, Nevada Operations Office report DOE/NV-690-REV.1.
- DOE (U.S. Department of Energy), 2004. Surface Corrective Action Investigation Report with Surface Corrective Action Plan for the Gasbuggy Site, New Mexico, Nevada Site Office report DOE/NV-908.
- Dube, H.G., G.E. Chistiansen, J.H. Frantz, N.R. Fairchild, A.J. Olszewski, W.K. Sawyer, and J.R. Williamson, 2000. The Lewis Shale, San Juan Basin: What we know now, *SPE*

- 63091, paper prepared for the 2000 SPE Annual Technical Conference and Exhibition, Dallas, Texas, October 1-4, 2000.
- Frink, R.O., and J.A. Wethington, Jr., 1971. Tritium exchange between hydrocarbons and steam. Transactions of the American Nuclear Society, 1971 Winter Meeting, Miami Beach, pp. 467-468.
- Holzer, F., 1968. Gasbuggy Preliminary Postshot Summary Report, Lawrence Radiation Laboratory rpt. PNE-1003, p. 16.
- Holzer, A., 1970. Gasbuggy in Perspective. American Nuclear Society, Proceedings of Symposium on Engineering with Nuclear Explosives, 1:662-697.
- Horne, R.N., 1995. *Modern Well Test Analysis*, second ed. Petroway, Inc., p. 257.
- International Atomic Energy Agency (IAEA), 1998. The radiological situation at the atolls of Mururoa and Fangataufa. Technical Report in six volumes, Radiological assessment report series, Vienna, Austria.
- Jacobs, D.G., C.J. Barton, C.R. Bowman, G.R. Briggs, W.M. Culkowski, M.J. Kelly, P.S. Rohwer, and E.G. Struxness, 1971. Theoretical Evaluation of Consumer Products from Project Gasbuggy, Final Report, Phase I: Impact of Hypothetical Releases of Contaminated Gas in the San Juan Basin. Oak Ridge National Laboratory report ORNL-4646.
- Jury, W.A., W.R. Gardner, and W.H. Gardner, 1991, *Soil Physics*, 5th ed., Wiley, p. 328.
- Korver, J.A., and D.E. Rawson, 1968. Gasbuggy Postshot Investigations in GB-ER, Lawrence Radiation Laboratory Report UCRL-50425.
- Lorenz, J.C., and S.P. Cooper, 2003. Tectonic setting and characteristics of natural fractures in Mesaverde and Dakota reservoirs of the San Juan Basin, *New Mexico Geology*, New Mexico Bureau of Geology and Mineral Resources, 25(1), 3-14.
- Lucas, L.L., and M.P. Unterweger, 2000. Comprehensive review and critical evaluation of the half-life of tritium, *Journal of Research of the National Institute of Standards and Technology*, 105(4), July-August.
- Mercer, J.W., 1967. Technical Letter: Geology and Hydrology of Project Gasbuggy, Rio Arriba County, New Mexico, U.S. Geological Survey Technical Letter: Gasbuggy 4.
- Mercer, J.W., 1968. Inventory of Wells and Springs Within a 10-Mile Radius of Project Gasbuggy, Rio Arriba County, New Mexico, U.S. Geological Survey Open-File Report PNE-G-25.
- Pruess, K., 1991. TOUGH2—A General Purpose Numerical Simulator for Multiphase Fluid and Heat Flow. Lawrence Berkeley Laboratory Report LBL-29400, Berkeley, CA.
- Pruess, K., C. Oldenburg, and G. Moridis, 1999. TOUGH2 User's Guide, Version 2.0. Lawrence Berkeley Laboratory Report LBNL-43134, Berkeley, CA.
- Rawson, D.E., J.A. Korver, R.L. Pritchard, and W. Martin, 1968. Post-shot geologic Investigations—Project Gasbuggy, Lawrence Radiation Laboratory Report UCRL-71354.

- Reid, R.C., J.M. Prausnitz, and B.E. Poling, 1987. *The Properties of Gases and Liquids*, McGraw Hill, p. 74.
- Smith, C.F., 1970. Behavior of radionuclides in nuclear gas stimulation applications, in proc. Symposium Engineering with Nuclear Explosives, Las Vegas, Nevada Jan 14-16, 1970, AEC rpt. CONF700100, pp. 818-830.
- Smith, D.K., B.K. Esser, and J.L. Thompson, 1995. Uncertainties Associated with the Definition of a Hydrologic Source Term for the Nevada Test Site. Lawrence Livermore National Laboratory Report UCRL-ID-120322, p. 21.
- Stone, W.J., F.P. Lyford, P.F. Frenzel, N.H. Mizell, and E.T. Padgett, 1983. Hydrogeology and Water Resources of San Juan Basin, New Mexico, New Mexico Bureau of Mines and Mineral Resources Hydrologic Report 6.
- Tewes, 1979. Survey of gas quality results from three gas-well-stimulation experiments by nuclear explosions. Lawrence Livermore Laboratory rpt. UCRL-52656, p. 34.
- Thomas, R.D., and D.C. Ward, 1972. Effect of overburden pressure and water saturation gas permeability of tight sandstone cores. *Journal of Petroleum Technology*, v. 24, February, pp. 120-124.
- Tompson, A.F.B., C.J. Bruton, and G.A. Pawloski, 1999. Evaluation of the Hydrologic Source Term from Underground Nuclear Tests in Frenchman Flat at the Nevada Test Site: The Cambic Test, Lawrence Livermore National Laboratory Report UCRL-ID-132300, p. 319.
- van Genuchten, R., 1980. A closed-form equation for predicting the hydraulic conductivity of unsaturated soils. *Soil Science Society of America Journal*, 44(5), 892-898.
- Ward, D.C., and R.F. Lemon, 1968. Status of reservoir evaluation Project Gasbuggy, paper presented at SPE Fall meeting, Houston, Sept. 29, 1968, also PNE-G-13, p. 31.
- Wethington, J.A., Jr., 1970. Possible techniques for decontamination of natural gas from gas wells stimulated by a nuclear explosion. *In American Nuclear Society and U.S. Atomic Energy Agency, Proceedings from Symposium on Engineering with Nuclear Explosives, Las Vegas, Nevada, CONF-700101, Vol. 2., pp. 1589-1596.*

## APPENDIX: TOUGH2 V2.0 Governing Equations

The two fluid phases are gas (water vapor and air) and liquid water. The governing mass and heat transport equations are:

$$\frac{d}{dt} \int_{V_n} M^\kappa dV_n = \int_{\Gamma_n} \mathbf{F}^\kappa \cdot \mathbf{n} d\Gamma_n + \int_{V_n} q^\kappa dV_n \quad (\text{A1})$$

where the integration is over the domain of the flow system,  $V_n$ , which is bounded by the closed surface  $\Gamma_n$ . The quantity  $M$  that appears in the accumulation term represents mass or energy per unit volume, where the components (mass and/or heat) are labeled by  $\kappa$  ( $\kappa=1$  water,  $\kappa=2$  air,  $\kappa=3$  heat).  $\mathbf{F}$  denotes mass or heat flux and  $q$  denotes sources and sinks. The normal vector  $\mathbf{n}$  on the surface  $d\Gamma_n$  points inward into  $V_n$ .

The mass accumulation term is:

$$M^\kappa = \phi \sum_{\beta} S_{\beta} \rho_{\beta} X_{\beta}^{\kappa} \quad (\text{A2})$$

The total mass of component  $\kappa$  is obtained by summing over the fluid phases  $\beta$  (liquid, gas),  $\phi$  is porosity,  $S_{\beta}$  is saturation of phase  $\beta$ ,  $\rho_{\beta}$  is the density of phase  $\beta$ , and  $X_{\beta}^{\kappa}$  is the mass fraction of component  $\kappa$  in phase  $\beta$ . The heat accumulation term is:

$$M^3 = (1 - \phi) \rho_r C_r T + \phi \sum_{\beta} S_{\beta} \rho_{\beta} u_{\beta} \quad (\text{A3})$$

where  $\rho$  is the grain density of the porous medium,  $C_r$  is the specific heat of the rock,  $T$  is temperature, and  $u_{\beta}$  is the internal energy of phase  $\beta$ .

Mass flux terms are summed over the two mobile phases:

$$\mathbf{F}^\kappa = \sum_{\beta} X_{\beta}^{\kappa} \mathbf{F}_{\beta}^{\kappa} \quad (\text{A4})$$

and the flux of each phase is modeled by the multiphase version of Darcy's law:

$$\mathbf{F}_{\beta} = \rho_{\beta} \mathbf{u}_{\beta} = -k \frac{k_{r\beta} \rho_{\beta}}{\mu_{\beta}} (\nabla P_{\beta} + \rho_{\beta} \mathbf{g}) \quad (\text{A5})$$

Here,  $\mathbf{u}_{\beta}$  is the Darcy velocity of phase  $\beta$ ,  $k$  is absolute permeability,  $k_{r\beta}$  is the relative permeability to phase  $\beta$ ,  $\mu_{\beta}$  is the dynamic viscosity of phase  $\beta$ , and  $\nabla P_{\beta}$  is the pressure gradient across phase  $\beta$ .

Heat flux (conduction and convection) is:

$$\mathbf{F}^3 = -\lambda \nabla T + \sum_{\beta} h_{\beta} \mathbf{F}_{\beta} \quad (\text{A6})$$

where  $\lambda$  is thermal conductivity, and  $h_{\beta}$  is the specific enthalpy of phase  $\beta$ .

Mass diffusion for both solutes and gases is modeled with Fick's law:

$$\mathbf{f}_\beta^\kappa = -\phi\tau_o\tau_\beta\rho_\beta D_\beta^\kappa \nabla X_\beta^\kappa \quad (\text{A7})$$

where  $\mathbf{f}_\beta^\kappa$  is the mass flux of component  $\kappa$  in phase  $\beta$ ,  $\phi$  is porosity,  $\tau_o$  a tortuosity parameter dependent on pore geometry,  $\tau_\beta$  is a tortuosity parameter dependent on phase saturation,  $D_\beta^\kappa$  is the diffusion coefficient of component  $\kappa$  in phase  $\beta$ , and  $X_\beta^\kappa$  is the mass fraction of component  $\kappa$  in phase  $\beta$ . The hydrodynamic dispersion module available in TOUGH2 was not implemented in these simulations. There are no data on dispersivities and because properties of the fractures themselves are largely unknown, dispersion would only contribute to uncertainty. Fortunately, the primary interest is in radionuclide transport in the gas phase and unlike the case for liquids, mass flux due to gas diffusion in porous media and fractures is more important than gas dispersion. This is explained in the text using a scale analysis.

## DISTRIBUTION LIST

Jalena Dayvault  
Office of Legacy Management  
U.S. Department of Energy  
2597 Legacy Way  
Grand Junction, CO 81503  
Jalena.Dayvault@lm.doe.gov

Richard Hutton  
Stoller  
2597 Legacy Way  
Grand Junction, CO 81503  
Rick.Hutton@lm.doe.gov

Jenny Chapman  
Desert Research Institute  
755 E. Flamingo Road  
Las Vegas, NV 89119-7363  
Jenny.Chapman@dri.edu

\*Nevada State Library and Archives  
State Publications  
100 North Stewart Street  
Carson City, NV 89701-4285

Archives Getchell Library  
University of Nevada, Reno  
1664 N. Virginia St.  
Reno, NV 89557  
dcurtis@unr.edu

DeLaMare Library  
Mail Stop 262  
University of Nevada, Reno  
1664 N. Virginia St.  
Reno, NV 89557  
dcurtis@unr.edu

Document Section, Library  
University of Nevada, Las Vegas  
4505 Maryland Parkway  
Las Vegas, NV 89154  
sue.waincott@unlv.edu

†Library  
Southern Nevada Science Center  
Desert Research Institute  
755 E. Flamingo Road  
Las Vegas, NV 89119-7363

‡Nuclear Testing Archive  
ATTN: Martha DeMarre  
National Security Technologies, LLC  
Mail Stop 400  
PO Box 98521  
Las Vegas, NV 89193-8521  
demarrme@nv.doe.gov  
(2 CDs)

§Office of Scientific and Technical Information  
U.S. Department of Energy  
P.O. Box 62  
Oak Ridge, TN 37831-9939

*All on distribution list receive one electronic PDF copy, unless otherwise noted.*

---

\* 12 paper copies

† 3 paper copies; CD with pdf (from which to print)

‡ compact disc only

§ electronic copy (pdf) only